A SECOND-ORDER ENERGY STABLE BDF NUMERICAL SCHEME FOR THE CAHN-HILLIARD EQUATION

YUE YAN*, WENBIN CHEN†, CHENG WANG‡, AND STEVEN M. WISE§

Abstract. In this paper we present a second order accurate (in time) energy stable numerical scheme for the Cahn-Hilliard (CH) equation, with a mixed finite element approximation in space. Instead of the standard second order Crank-Nicolson methodology, we apply the implicit backward differentiation formula (BDF) concept to derive second order temporal accuracy, but modified so that the concave diffusion term is treated explicitly. This explicit treatment for the concave part of the chemical potential ensures the unique solvability of the scheme without sacrificing energy stability. An additional term $A\tau\Delta(u^{k+1}-u^k)$ is added, which represents a second order Douglas-Dupont-type regularization, and a careful calculation shows that energy stability is guaranteed, provided the mild condition $A \geq \frac{1}{16}$ is enforced. In turn, a uniform in time H^1 bound of the numerical solution becomes available. As a result, we are able to establish an $\ell^\infty(0,T;L^2)$ convergence analysis for the proposed fully discrete scheme, with full $O(\tau^2+h^2)$ accuracy. This convergence turns out to be unconditional; no scaling law is needed between the time step size τ and the spatial grid size h. A few numerical experiments are presented to conclude the article.

Key words. Cahn-Hilliard equation, energy stable BDF, Douglas-Dupont regularization, mixed finite element, energy stability

AMS subject classifications. 35K35, 35K55, 65M12, 65M60

1. Introduction.

The Allen-Cahn (AC) [1] (non-conserved dynamics) and Cahn-Hilliard (CH) [7] (conserved dynamics) equations, which model spinodal decomposition in a binary alloy, are perhaps the most well-known of the gradient flow-type PDEs. In deriving the CH equation, we consider a bounded domain $\Omega \subset \mathbb{R}^d$ (with $d=2$ or $d=3$). For any $u \in H^1(\Omega)$, the CH energy functional is given by

$$E(u) = \int_\Omega \left(\frac{1}{4}u^4 - \frac{1}{2}u^2 + \frac{\varepsilon^2}{2}|\nabla u|^2 \right) d\mathbf{x}, \tag{1.1}$$

where ε is a positive constant that dictates the interface width. (See [7] for a detailed derivation.) The CH equation is precisely the H^{-1} (conserved) gradient flow of the energy functional (1.1):

$$\begin{cases} u_t = \Delta w, \quad \text{in} \quad \Omega \times (0,T), \\ w := \delta_\phi E = u^3 - u - \varepsilon^2 \Delta u, \quad \text{in} \quad \Omega \times (0,T), \\ \partial_n u = \partial_n w = 0, \quad \text{on} \quad \partial\Omega \times (0,T), \\ u(\,\cdot\,,0) = u_0, \quad \text{in} \quad \Omega, \end{cases} \tag{1.2}$$

where $T>0$ is the final time, which may be infinite; $\partial_n u := \boldsymbol{n} \cdot \nabla u$; and $\boldsymbol{n}$ the unit normal vector on the boundary. Due to the gradient structure of (1.2), the following energy dissipation law holds:

$$\frac{d}{dt}E(u(t)) = -\int_\Omega |\nabla w|^2 d\mathbf{x}. \tag{1.3}$$

*School of Mathematical Sciences; Fudan University, Shanghai, China 200433 (yanyue@fudan.edu.cn)

†School of Mathematical Sciences; Fudan University, Shanghai, China 200433 (wbchen@fudan.edu.cn)

‡Mathematics Department; University of Massachusetts; North Dartmouth, MA 02747, USA (corresponding author: cwang1@umassd.edu)

§Mathematics Department; University of Tennessee; Knoxville, TN 37996, USA (swise1@utk.edu)

In integral form, the energy decay may be expressed as

$$E(u(t_1)) + \int_{t_0}^{t_1} \int_{\Omega} |\nabla w(t)|^2 d\mathbf{x} dt = E(u(t_0)). \tag{1.4}$$

Furthermore, the equation is mass conservative, $\int_{\Omega} \partial_t u \, d\mathbf{x} = 0$, which follows from the conservative structure of the equation together with the homogeneous Neumann boundary conditions for w. This property can be re-expressed as $(u(\cdot, t), 1) = (u_0, 1)$, for all $t \geq 0$.

The Cahn-Hilliard equation is one of the most important models in mathematical physics. It is often paired with equations that describe important physical behavior of a given physical system, typically through nonlinear coupling terms. Examples of such coupled models include the Cahn-Hilliard-Navier-Stokes (CHNS) equation for two-phase, immiscible flow; the Cahn-Larché model of binary solid state diffusion for elastic misfit; the Cahn-Hilliard-Hele-Shaw (CHHS) equation for spinodal decomposition of a binary fluid in a Hele-Shaw cell; et cetera. The numerical and PDE analyses for the CH equation are quite challenging, since the equation is a fourth-order, nonlinear parabolic-type PDE. There have been many existing numerical works, in particular for first order accurate (in time) schemes.

Meanwhile, second order accurate (in time) numerical schemes have also attracted a great deal of attention in recent years, due to the great advantage over their first order counterparts in terms of numerical efficiency and accuracy. However, the analysis for the second order schemes is significantly more difficult than that for the first order ones, because of the more complicated form for the nonlinear terms; see the related discussions in [2, 21, 24], et cetera.

The energy stability of a numerical scheme has been a very important issue, since it plays an essential role in the accuracy of long time numerical simulation. The standard convex splitting scheme, popularized by Eyre's work [17], is a well-known approach to achieve numerical energy stability. This framework treats the convex part of the chemical potential implicitly and the concave part explicitly, resulting in a scheme that is uniquely solvable and energy stable, unconditionally with respect to the time and space step sizes. Splitting has been applied to a wide class of gradient flows in recent years, and both first and second order accurate (in time) algorithms have been developed. See the related works for the phase field crystal (PFC) equation and the modified phase field crystal (MPFC) equation [3, 4, 28, 35, 37]; epitaxial thin film growth models [8, 10, 32, 34]; non-local Cahn-Hilliard-type models [22, 23]; the CHHS and related models [9, 13, 20, 36]; et cetera. One drawback of the first order convex splitting approach, however, is that the extra dissipation added to ensure unconditional stability also introduces a significant amount of numerical error [12]. For this reason, second-order energy stable methods have been highly desirable.

Recently, for the CH equation (1.2), a second order energy stable scheme has been analyzed in [25], based on a modified version of the Crank-Nicolson temporal approximation; see the related discussions in Remarks 2.1 and 4.3. This numerical scheme enjoys many advantages over the second order temporal approximations reported in the existing literature [5, 16, 24, 38], in particular in terms of the unconditional energy stability, unconditionally unique solvability, and rigorous convergence properties. See also the recent finite element work [15] for related analysis; and see the extension of the ideas in [15, 25] to the Cahn-Hilliard-Navier-Stokes model in the recent papers [14, 27].

In this paper, we propose and analyze an alternate second order energy stable

scheme for the CH equation (1.2), based on the 2nd order BDF temporal approximation framework, instead of that based on the Crank-Nicolson one. The BDF scheme treats and approximates every term at the time step t^{n+1} (instead of the time instant $t^{n+1/2}$). In more detail, a 2nd order BDF 3-point stencil is applied in the temporal derivative approximation, and the nonlinear term and the surface diffusion terms are updated implicitly, due to their strong convexities. Meanwhile, a second order accurate, explicit extrapolation formula has to be applied in the approximation of the concave diffusion term, in order to make the numerical scheme uniquely solvable.

However, the energy stability is not assured for this explicit extrapolation, by a direct calculation. To salvage the energy stability of the numerical scheme, we add a second order Douglas-Dupont regularization, in the form of $A\tau\Delta(u^{k+1} - u^k)$. A more careful analysis then guarantees the energy stability for this proposed numerical scheme under a mild requirement $A \geq \frac{1}{16}$. For the present scheme, we highlight the fact that the nonlinear solver required for the BDF scheme is expected to require **less** computational effort than that for the Crank-Nicolson version, due to the simpler form and stronger convexity properties of the nonlinear term.

A mixed finite element approximation is taken in space, based on a mixed weak formulation of the CH equation (1.2). In this approach, the numerical solutions for both the phase variable u and the chemical potential variable w belong to the same finite element space S_h, which is a piecewise polynomial subspace of H^1. Combined with the second order energy stable BDF temporal approximation, the resulting numerical scheme preserves the properties of unique solvability and unconditional energy stability. In turn, a uniform-in-time H^1 bound can be derived for the numerical phase variable u_h. With a help of this uniform-in-time H^1 bound, we are able to establish the convergence analysis, with a combination of consistency and stability estimates for the numerical error functions. The error estimate, in the $\ell^\infty(0,T;L^2)\cap\ell^2(0,T;H_h^2)$ norm, has the full order $O(\tau^2+h^2)$ accuracy. Furthermore, this convergence is unconditional; no scaling law is needed between τ and h to ensure its validity.

This article is organized as follows. In Section 2 we outline the fully discrete scheme. The unique solvability is proven in Section 3 and the energy stability analysis is established in Section 4. In Section 5 we present the $\ell^\infty(0,T;L^2)\cap\ell^2(0,T;H_h^2)$ convergence analysis for the scheme. Some numerical results are presented in Section 6. Finally, concluding remarks are given in Section 7.

2. The fully discrete numerical scheme. We use standard notation for the norms on their respective function spaces. In particular, we denote the standard norms for the Sobolev spaces $W^{m,p}(\Omega)$ by $\|\cdot\|_{m,p}$. We replace $\|\cdot\|_{0,p}$ by $\|\cdot\|_p$, $\|\cdot\|_{0,2} = \|\cdot\|_2$ by $\|\cdot\|$, and $\|\cdot\|_{q,2}$ by $\|\cdot\|_{H^q}$.

The mixed weak formulation of Cahn-Hilliard equation (1.2) is to find $u, w \in L^2(0,T;H^1(\Omega))$, with $u_t \in L^2(0,T;H^{-1}(\Omega))$, satisfying

$$\begin{cases} (u_t, v) + (\nabla w, \nabla v) = 0, & \forall\ v \in H^1(\Omega), \\ (w,\psi) = (u^3 - u, \psi) + \varepsilon^2(\nabla u, \nabla\psi), & \forall\ \psi \in H^1(\Omega), \end{cases} \tag{2.1}$$

for almost every $t \in [0,T]$, where $H^{-1}(\Omega)$ is the dual space of $H^1(\Omega)\cap L_0^2(\Omega)$, where $L_0^2(\Omega) := \{u \in L^2(\Omega) \mid (u,1) = 0\}$, and $(\cdot,\cdot)$ represents the L^2 inner product or the duality pairing, as appropriate.

Let $\mathcal{T}_h = \{K\}$ be a quasi-uniform triangulation on Ω. For $q \in \mathbb{Z}^+$, define the piecewise polynomial space $S_h := \{v \in C^0(\Omega) \mid v|_K \in \mathcal{P}_q(K), \forall\ K \in \mathcal{T}_h\} \subset H^1(\Omega)$.

We propose the following fully discrete numerical scheme: for $n \geq 1$, given $u_h^{n-1}, u_h^n \in S_h$, find $u_h^{n+1}, w_h^{n+1} \in S_h$, such that

$$\begin{cases} \left(\dfrac{3u_h^{n+1} - 4u_h^n + u_h^{n-1}}{2\tau}, v_h\right) + (\nabla w_h^{n+1}, \nabla v_h) = 0, \qquad \forall\ v_h \in S_h, \\ (w_h^{n+1}, \psi_h) = \varepsilon^2(\nabla u_h^{n+1}, \nabla \psi_h) + ((u_h^{n+1})^3 - 2u_h^n + u_h^{n-1}, \psi_h) \\ \qquad\qquad + A\tau(\nabla(u_h^{n+1} - u_h^n), \nabla \psi_h), \qquad \forall\ \psi_h \in S_h, \end{cases} \tag{2.2}$$

where u_h^n stands for the numerical solution at time t_n. As a general rule, the second order Gear method (BDF approximation) is expected to yield a large region of absolute stability. The explicit Adams-Bashforth extrapolation formula (with a second order approximation to the variable at time step t^{n+1}) is applied to stabilize the concave term, as we will show. The artificial term $A\tau\Delta(u_h^{n+1} - u_h^n)$ – a second order-accurate Douglas-Dupont-type regularization – is added to establish the *unconditional energy stability* of the scheme, provided A is sufficiently large, while preserving the second order temporal accuracy and unique solvability of the scheme. We will show that, there is only a very mild stability requirement on the artificial parameter A, namely, $A \geq \frac{1}{16}$.

The scheme requires an initialization step. To this end, we introduce the Ritz projection operator $R_h : H^1(\Omega) \to S_h$, satisfying

$$(\nabla(R_h\varphi - \varphi), \nabla\chi) = 0, \quad \forall \chi \in S_h, \qquad (R_h\varphi - \varphi, 1) = 0. \tag{2.3}$$

The initial data are chosen so that $u_h^0 = R_h u_0$. Then, we use a standard first-order energy stable method to obtain $u_h^1, w_h^1 \in S_h$. Precisely, the initialization step is as follows: given $u_h^0 \in S_h$, find $u_h^1, w_h^1 \in S_h$, such that

$$\begin{cases} \left(\dfrac{u_h^1 - u_h^0}{\tau}, v_h\right) + (\nabla w_h^1, \nabla v_h) = 0, \qquad \forall\ v_h \in S_h, \\ (w_h^1, \psi_h) = \varepsilon^2(\nabla u_h^1, \nabla \psi_h) + ((u_h^1)^3 - u_h^0, \psi_h), \qquad \forall\ \psi_h \in S_h, \end{cases} \tag{2.4}$$

We must solve a nonlinear algebraic system at every time step in the computation. However, many nonlinear solvers, such as the Newton's iteration or nonlinear conjugate gradient algorithm, and the nonlinear multigrid give robust performance, since the implicit part turns out to be the gradient of a certain strictly convex functional.

REMARK 2.1. *The Crank-Nicolson version of the second order convex splitting scheme for the CH equation* (1.2) *takes the (spatially-continuous) form:*

$$\begin{aligned} \frac{u^{n+1} - u^n}{\tau} &= \Delta w^{n+1/2}, \\ w^{n+1/2} &= \chi(u^{n+1}, u^n) - \left(\frac{3}{2}u^n - \frac{1}{2}u^{n-1}\right) - \varepsilon^2\Delta\left(\frac{3}{4}u^{n+1} + \frac{1}{4}u^{n-1}\right), \\ \chi(u^{n+1}, u^n) &:= \frac{1}{4}(u^{n+1} + u^n)\left((u^{n+1})^2 + (u^n)^2\right). \end{aligned} \tag{2.5}$$

See the detailed derivations and analyses in [11, 15, 25], involving finite difference, finite element and Fourier pseudo-spectral discretizations, respectively. In this numerical approach, every term in the chemical potential is approximated at the time instant $t^{n+1/2}$: A modified implicit second order approximation is employed for the highest-order diffusion term in order to preserve a stronger stability than the standard

Crank-Nicolson treatment; a second order explicit extrapolation is employed for the concave term; and, a modified Crank-Nicolson approximation (a secant approximation) is used on the nonlinear term.

We see that both the Crank-Nicolson version (2.5) *and the BDF one* (2.2) *require a nonlinear solver, while the nonlinear term in* (2.5) *takes a more complicated form than* (2.2)*, which comes from different time instant approximations. Moreover, a stronger convexity of the nonlinear term in the BDF one* (2.2) *improves the numerical efficiency in the nonlinear iteration. In turn, the nonlinear iteration solver in the proposed scheme* (2.2) *is expected to incur less computational cost than that for* (2.5)*. More detailed comparison between these two different second order energy stable approaches will be given in Remarks 4.3, 4.4.*

3. Unique solvability. To facilitate the analysis below, we define the discrete Laplacian operator and the discrete H^{-1} norm. We will make use of the notation $L_0^2(\Omega) := \big\{u \in L^2(\Omega) \;\big|\; (u,1) = 0\big\}$, and, generically, if $V \subseteq L^2(\Omega)$, $\mathring{V} := L_0^2 \cap V$.

DEFINITION 3.1. *The discrete Laplacian operator $\Delta_h : S_h \to \mathring{S}_h$ is defined as follows: for any $v_h \in S_h$, $\Delta_h v_h \in \mathring{S}_h$ denotes the unique solution to the problem*

$$(\Delta_h v_h, \chi) = -(\nabla v_h, \nabla \chi), \qquad \forall\ \chi \in S_h.$$

It is straightforward to show that by restricting the domain, $\Delta_h : \mathring{S}_h \to \mathring{S}_h$ is invertible, and for any $v_h \in \mathring{S}_h$, we have

$$(\nabla(-\Delta_h)^{-1} v_h), \nabla\chi) = (v_h, \chi), \quad \forall\ \chi \in S_h.$$

LEMMA 3.1. *Let $u \in H_N^2(\Omega) := \big\{u \in H^2(\Omega) \;\big|\; \partial_n u = 0 \text{ on } \partial\Omega\big\}$. Then*

$$\|\Delta_h(R_h u)\| \le \|\Delta u\|\,. \tag{3.1}$$

Proof. Let $v_h \in S_h$ be arbitrary. Then

$$-(\Delta u, v_h) = (\nabla u, \nabla v_h) = (\nabla(R_h u), \nabla v_h) = -(\Delta_h(R_h u), v_h). \tag{3.2}$$

Thus, setting $v_h = -\Delta_h(R_h u)$, we have, by the Cauchy-Schwarz inequality,

$$\|\Delta_h(R_h u)\|^2 = (\Delta u, \Delta_h(R_h u)) \le \|\Delta u\| \cdot \|\Delta_h(R_h u)\|\,. \tag{3.3}$$

In turn, the result follows on dividing by $\|\Delta_h(R_h u)\|$. ∎

DEFINITION 3.2. *The discrete H^{-1} norm, $\|\cdot\|_{-1,h}$, is defined as follows:*

$$\|v_h\|_{-1,h} := \sqrt{(v_h, (-\Delta_h)^{-1} v_h)}, \quad \forall v_h \in \mathring{S}_h.$$

Now, suppose $\psi_h \in \mathring{S}_h$ and take the test function as $v_h = (-\Delta_h)^{-1}\psi_h$ in our mixed scheme (2.2), we obtain

$$\begin{aligned}\left(\frac{3u_h^{n+1} - 4u_h^n + u_h^{n-1}}{2\tau}, (-\Delta_h)^{-1}\psi_h\right) + \varepsilon^2(\nabla u_h^{n+1}, \nabla\psi_h)\\ +((u_h^{n+1})^3 - 2u_h^n + u_h^{n-1}, \psi_h) + A\tau(\nabla(u_h^{n+1} - u_h^n), \nabla\psi_h) = 0.\end{aligned} \tag{3.4}$$

By rearranging the above equation, we get, for every $\psi_h \in \mathring{S}_h$,

$$((u_h^{n+1})^3 - (A\tau + \varepsilon^2)\Delta_h u_h^{n+1} + \frac{3}{2\tau}(-\Delta_h)^{-1}(u_h^{n+1} - \bar{u}), \psi_h) = f[u_h^n, u_h^{n-1}](\psi_h), \tag{3.5}$$

where $f[u_h^n, u_h^{n-1}]$ is a bounded linear functional involving the previous time iterates and $\bar{u}$ is the time-invariant mass average of u_h^k. We make the transformation $q_h = u_h^{k+1} - \bar{u} \in \mathring{S}_h$. Then $q_h \in \mathring{S}_h$ satisfies

$$((q_h + \bar{u})^3 - (A\tau + \varepsilon^2)\Delta_h q_h + \frac{3}{2\tau}(-\Delta_h)^{-1} q_h, \psi_h) = f[u_h^n, u_h^{n-1}](\psi_h), \tag{3.6}$$

iff $u_h^{k+1} \in \mathring{S}_h$ satisfies (3.5). Define

$$G(q_h) := \frac{1}{4}\|q_h + \bar{u}\|_4^4 + \frac{1}{2}(A\tau + \varepsilon^2)\|\nabla q_h\|^2 + \frac{3}{4\tau}\|q_h\|_{-1,h}^2 - f[u_h^n, u_h^{n-1}](q_h).$$

Since $G(\,\cdot\,)$ is a strictly convex functional over the admissible set $\mathring{S}_h$, it has a unique minimizer. The unique minimizer, $q_h \in \mathring{S}_h$, satisfies the Euler-Lagrange equation, which coincides with the variational problem (3.6). By equivalence, the solution to (3.4) exists and is unique. The unique solvability of the initialization scheme (2.4) is similar. See, for example, [13].

4. Energy stability and a uniform-in-time H^1 stability. The following energy stability estimate is available.

THEOREM 4.1. *For $n \geq 1$, define*

$$\mathcal{E}(u_h^{n+1}, u_h^n) := E(u_h^{n+1}) + \frac{1}{4\tau}\|u_h^{n+1} - u_h^n\|_{-1,h}^2 + \frac{1}{2}\|u_h^{n+1} - u_h^n\|^2, \tag{4.1}$$

and suppose $A \geq \frac{1}{16}$. Then the numerical scheme (2.2) *has the energy-decay property*

$$\mathcal{E}(u_h^{n+1}, u_h^n) + \tau\left(1 - \frac{1}{16A}\right)\left\|\frac{u_h^{n+1} - u_h^n}{\tau}\right\|_{-1,h}^2 \leq \mathcal{E}(u_h^n, u_h^{n-1}). \tag{4.2}$$

Proof. In (2.2), taking $v_h = (-\Delta_h)^{-1}(u_h^{n+1} - u_h^n)$ and $\psi_h = u_h^{n+1} - u_h^n$, the two terms including w_h cancel out each other by the definition of Δ_h. Therefore,

$$\begin{aligned} 0 &= \frac{1}{2\tau}(3u_h^{n+1} - 4u_h^n + u_h^{n-1}, -\Delta_h^{-1}(u_h^{n+1} - u_h^n)) + \varepsilon^2(\nabla u_h^{n+1}, \nabla(u_h^{n+1} - u_h^n)) \\ &\quad + ((u_h^{n+1})^3, u_h^{n+1} - u_h^n) - (2u_h^n - u_h^{n-1}, u_h^{n+1} - u_h^n) + A\tau\|\nabla(u_h^{n+1} - u_h^n)\|^2 \\ &:= J_1 + J_2 + J_3 + J_4 + J_5. \end{aligned}$$

We establish now establish estimates for $J_1, \cdots, J_5$. The time difference term becomes

$$\begin{aligned} J_1 &= \frac{1}{2\tau}(3u_h^{n+1} - 4u_h^n + u_h^{n-1}, -\Delta_h^{-1}(u_h^{n+1} - u_h^n)) \\ &= \tau\left(\frac{5}{4}\left\|\frac{u_h^{n+1} - u_h^n}{\tau}\right\|_{-1,h}^2 - \frac{1}{4}\left\|\frac{u_h^n - u_h^{n-1}}{\tau}\right\|_{-1,h}^2\right) \\ &\quad + \frac{\tau^3}{4}\left\|\frac{u_h^{n+1} - 2u_h^n + u_h^{n-1}}{\tau^2}\right\|_{-1,h}^2. \end{aligned} \tag{4.3}$$

The highest-order diffusion term turns out to be

$$\begin{aligned} J_2 &= \varepsilon^2(\nabla u_h^{n+1}, \nabla(u_h^{n+1} - u_h^n)) \\ &= \frac{\varepsilon^2}{2}\left(\|\nabla u_h^{n+1}\|^2 - \|\nabla u_h^n\|^2\right) + \frac{\varepsilon^2}{2}\left\|\nabla(u_h^{n+1} - u_h^n)\right\|^2. \end{aligned} \tag{4.4}$$

For the nonlinear term, we have

$$J_3 = ((u_h^{n+1})^3, u_h^{n+1} - u_h^n) = \frac{1}{4}\left(\|u_h^{n+1}\|_{L^4}^4 - \|u_h^n\|_{L^4}^4\right) + \frac{1}{4}\left\|(u_h^{n+1})^2 - (u_h^n)^2\right\|^2 + \frac{1}{2}\left\|u_h^{n+1}(u_h^{n+1} - u_h^n)\right\|^2. \tag{4.5}$$

For the concave diffusive term, we have

$$\begin{aligned} J_4 = & -(2u_h^n - u_h^{n-1}, u_h^{n+1} - u_h^n) = -(u_h^n, u_h^{n+1} - u_h^n) - (u_h^n - u_h^{n-1}, u_h^{n+1} - u_h^n) \\ = & -\frac{1}{2}\left(\|u_h^{n+1}\|^2 - \|u_h^n\|^2\right) + \frac{1}{2}\|u_h^{n+1} - u_h^n\|^2 \\ & + (u_h^{n+1} - 2u_h^n + u_h^{n-1}, u_h^{n+1} - u_h^n) - \left\|u_h^{n+1} - u_h^n\right\|^2 \\ = & -\frac{1}{2}\|u_h^{n+1}\|^2 + \frac{1}{2}\left\|u_h^{n+1} - u_h^n\right\|^2 - \left(-\frac{1}{2}\|u_h^n\|^2 + \frac{1}{2}\left\|u_h^n - u_h^{n-1}\right\|^2\right) \\ & + \frac{1}{2}\left\|u_h^{n+1} - 2u_h^n + u_h^{n-1}\right\|^2 - \frac{1}{2}\left\|u_h^{n+1} - u_h^n\right\|^2. \end{aligned} \tag{4.6}$$

Finally, for the stabilizing term, we have

$$J_5 = A\tau\|\nabla(u_h^{n+1} - u_h^n)\|^2.$$

Using the Cauchy-Schwarz inequality, for any $\alpha > 0$,

$$\begin{aligned} \frac{1}{2}\|u_h^{n+1} - u_h^n\|^2 &\le \frac{1}{2}\left\|\nabla u_h^{n+1} - \nabla u_h^n\right\| \cdot \|u_h^{n+1} - u_h^n\|_{-1,h} \\ &\le \frac{\tau}{4\alpha}\left\|\nabla u_h^{n+1} - \nabla u_h^n\right\|^2 + \frac{\alpha\tau}{4}\left\|\frac{u_h^{n+1} - u_h^n}{\tau}\right\|_{-1,h}^2. \end{aligned} \tag{4.7}$$

Putting everything together, we have

$$\begin{aligned} \mathcal{E}(u_h^{n+1}, u_h^n) \ & + \tau\left(1 - \frac{\alpha}{4}\right)\left\|\frac{u_h^{n+1} - u_h^n}{\tau}\right\|_{-1,h}^2 \\ & + \tau\left(A - \frac{1}{4\alpha}\right)\|\nabla(u_h^{n+1} - u_h^n)\|^2 \le \mathcal{E}(u_h^n, u_h^{n-1}), \end{aligned}$$

where the numerical energy function $\mathcal{E}(u_h^{n+1}, u_h^n)$ is defined in (4.1). The result follows on setting $\alpha = \frac{1}{4A}$. ∎

We have the following well-known stability for the initialization scheme.

THEOREM 4.2. *The initialization scheme* (2.4) *has the energy-decay property*

$$E(u_h^1) + \tau\left\|\frac{u_h^1 - u_h^0}{\tau}\right\|_{-1,h}^2 \le E(u_h^0). \tag{4.8}$$

Since $\left\|\frac{u_h^1 - u_h^0}{\tau}\right\|_{-1,h} = \left\|\nabla w_h^1\right\|$, *this is equivalent to*

$$E(u_h^1) + \tau\left\|\nabla w_h^1\right\|^2 \le E(u_h^0). \tag{4.9}$$

REMARK 4.1. *A requirement for the artificial coefficient,* $A \geq \frac{1}{16}$*, ensures a modified energy stability at a theoretical level. On the other hand, this requirement may be more associated with theoretical justification than practical necessity. Several numerical experiments have shown that the non-increasing energy property is still observed even with a value of* $A < \frac{1}{16}$*; see the detailed numerical simulation results reported in Section 6.*

REMARK 4.2. *Due to the forms of the energy* (1.1) *and the dynamical equation* (1.2)*, the lower bound requirement for A is* ε*-independent:* $A \geq \frac{1}{16}$*. Meanwhile, if the temporal scale is multiplied by an* ε^{-1} *factor, so that the energy functional becomes* $E(u) = \varepsilon^{-1}(\frac{1}{4}\|u\|_{L^4}^4 - \frac{1}{2}\|u\|^2) + \frac{\varepsilon}{2}\|\nabla u\|^2$*, as analyzed in [19, 33], a careful calculation indicates an* ε*-dependent requirement:* $A \geq \frac{1}{16}\varepsilon^{-2}$*, to ensure a modified energy stability in a similar form as* (4.2)*.*

REMARK 4.3. *The Crank-Nicolson scheme* (2.5)*, reported in [11, 15, 25], has also been proven to be uniquely solvable and unconditionally energy stable, combined with either the finite difference or mixed finite element spatial approximation. In particular, it is observed that no additional regularization term is needed for this scheme, in contrast with the proposed BDF scheme* (2.2)*. The reason for this difference comes from the subtle fact that the explicit treatment for the concave term in* (2.5)*, namely* $\frac{3}{2}u^n - \frac{1}{2}u^{n-1}$ *(a second order approximation to u at* $t^{n+1/2}$*), leads to the following stability estimate:*

$$(-\frac{3}{2}u^n + \frac{1}{2}u^{n-1}, u^{n+1} - u^n) \geq -\frac{1}{2}(\|u^{n+1}\|^2 - \|u^n\|^2) + \frac{1}{4}(\|u^{n+1} - u^n\|^2 - \|u^n - u^{n-1}\|^2). \tag{4.10}$$

In contrast, equality (4.6) *(for the BDF scheme) contains a negative term in the energy estimate:* $-\frac{1}{2}\|u_h^n - u_h^{n-1}\|^2$*. Consequently, an artificial term associated with Douglas-Dupont regularization is needed to balance this negative part, in order to establish the energy stability at a theoretical level.*

REMARK 4.4. *We have performed a numerical test to justify the expected improvement in numerical efficiency of the proposed BDF scheme* (2.2)*, with respect to the energy stable Crank-Nicolson scheme* (2.5)*, as argued in Remark 2.1. An exact numerical solution is set over a domain* $\Omega = (0,1)^2$*, with the physical parameter* $\varepsilon = 0.05$*, the spatial resolution* $h = \frac{1}{512}$*, and time step size* $\tau = 0.01$*. The preconditioned steepest descent (PSD) algorithm, proposed and analyzed in a more recent article [18], is applied to implement both numerical schemes, with the same initial guess in the nonlinear iterations.*

This numerical comparison is performed on an Apple iMac computer, with an Intel Core i6, 2.9 GHz processor, and 32 GB of 1600 MHz DDR3 memory. Our numerical experiments show that, it took 11 iterations for the BDF scheme (2.2) *to obtain an error tolerance of* 10^{-12} *(in the maximum norm), with 0.4042 seconds CPU time, while the Crank-Nicolson version* (2.5) *requires 14 iterations to obtain the same level of error tolerance, with 0.5263 seconds CPU time. As a result, we conclude that, since the nonlinear term in* (2.2) *has a stronger convexity than the one in* (2.5)*, a 20 to 25 percent improvement of the computational efficiency is generally expected.*

In addition to the proposed BDF scheme in this article and the Crank-Nicolson version [11, 14, 15, 25], there are a few related works with second-order in time approximations for the CH equation that we like to mention. A combination of an implicit midpoint rule and spatial discretization by the Fourier-Galerkin spectral method was introduced in a recent article [5]; the stabiliy estimates proved may

be viewed as conditional, there is a stability condition for τ in terms of the model parameters, although this restriction does not depend on h.

A semi-discrete second-order scheme for a family of Cahn-Hilliard-type equations was proposed in [38], with applications to diffuse interface tumor growth models. An unconditional energy stability was proved, by taking advantage of a (quadratic) cut-off of the double-well energy and artificial stabilization terms. And also, their scheme turns out to be linear, which is another advantage. However, a convergence analysis is not available in their work.

A careful examination of several second-order in time numerical schemes for the CH equation is presented in [24]. An alternate variable is used in the numerical design, denoted as a second order approximation to $v = u^2 - 1$. A linearized, second order accurate scheme is derived as the outcome of this idea, and an unconditional energy stability is established in a modified version. However, such an energy stability is applied to a pair of numerical variables (u, v), and an H^1 stability for the original physical variable u has not been justified. As a result, the convergence analysis is not available for this numerical approach. Similar methodology has been reported in the invariant energy quadratization (IEQ) approach [26, 39, 40, 41].

By combining all these observations, we note many advantages of the proposed BDF scheme and the Crank-Nicolson version over the second order temporal approximations reported in the existing literature, in particular in terms of the unconditional energy stability, unconditionally unique solvability and convergence analysis.

REMARK 4.5. *As an alternative to the nonlinear approaches, there has been a recent work of a linear BDF-type scheme in [30]:*

$$\frac{3u^{n+1} - 4u^n + u^{n-1}}{2\tau} = \Delta \left(2(u^n)^3 - (u^{n-1})^3 - (2u^n - u^{n-1}) - \varepsilon^2 \Delta u^{n+1}\right) - A\tau(-\Delta)^\alpha (u^{n+1} - u^n), \quad \text{with } \alpha = 0 \text{ or } 1. \tag{4.11}$$

The most important difference with our proposed BDF scheme (2.2) *is the purely explicit treatment for the nonlinear part of chemical potential, which in turn avoids a nonlinear solver. However, with this explicit update for the nonlinear term, a theoretical justification of the energy stability for* (4.11) *requires a coefficient A of the order $A = O(\varepsilon^{-36}|log\varepsilon|^{16})$ for $\alpha = 0$, and $A = O(\varepsilon^{-26}|log\varepsilon|^{12})$ for $\alpha = 1$. Also see the related analysis for the first order linear scheme [31]. In comparison, our proposed algorithm* (2.2) *only requires $A \geq \frac{1}{16}$ for the energy stability.*

Since the nonlinear part of the chemical potential $(u^{n+1})^3$ appears as a convex term in (2.2)*, either the nonlinear multigrid or Newton's iteration could be efficiently applied, and extensive numerical experiments have indicated a comparable computation cost as that for* (4.11)*.*

As a result of the stability estimate (4.2) for the numerical energy function (4.1), we are able to obtain an uniform-in-time H^1 estimate of the numerical solution:

THEOREM 4.3. *Suppose that the initial data are sufficiently regular that*

$$E(u_h^0) + \frac{1}{3}\left\|u_h^0\right\|^2 \leq \frac{C_0}{3},$$

for some C_0 that is independent of h, and $A \geq \frac{1}{16}$. Define $\kappa_A := 1 - \frac{1}{16A}$ and $\tilde{w}_h^{n+1} := \Delta_h^{-1}\left(\frac{u_h^{n+1} - u_h^n}{\tau}\right)$, for $n \geq 0$. Then, there are constants $C_1, C_2, C_3 > 0$, which

depend on C_0, Ω, and ε, but are independent of h and τ, such that for any $m \geq 1$

$$\|u_h^m\|_{H^1}^2 \leq C_1, \tag{4.12}$$

$$\tau \cdot \kappa_A \sum_{n=1}^{m} \left\| \frac{u_h^n - u_h^{n-1}}{\tau} \right\|_{-1,h}^2 = \tau \cdot \kappa_A \sum_{n=1}^{m} \|\nabla \tilde{w}_h^n\|^2 \leq C_2, \tag{4.13}$$

$$\tau \cdot \kappa_A \sum_{n=1}^{m} \|\nabla w_h^n\|^2 \leq C_3. \tag{4.14}$$

Proof. Since, for any $u \in L^4(\Omega)$, $\frac{1}{4}\|u\|_{L^4}^4 - \frac{1}{2}\|u\|^2 \geq \frac{1}{2}\|u\|^2 - |\Omega|$, it follows that

$$\frac{1}{2}\|u_h^n\|^2 + \frac{\varepsilon^2}{2}\|\nabla u_h^n\|^2 \leq E(u_h^n) + |\Omega|,$$

for any $n \geq 0$. From the stability of the initialization step (4.8) and using the triangle inequality, we have

$$\begin{aligned}
\mathcal{E}(u_h^1, u_h^0) &= E(u_h^1) + \frac{1}{4\tau}\|u_h^1 - u_h^0\|_{-1,h}^2 + \frac{1}{2}\|u_h^1 - u_h^0\|^2 \\
&\leq E(u_h^1) + \frac{1}{\tau}\|u_h^1 - u_h^0\|_{-1,h}^2 + \frac{1}{2}\|u_h^1 - u_h^0\|^2 \\
&\leq E(u_h^0) + \left\|u_h^1\right\|^2 + \left\|u_h^0\right\|^2 \\
&\leq E(u_h^0) + 2E(u_h^1) + 2|\Omega| + \left\|u_h^0\right\|^2 \\
&\leq 3E(u_h^0) + \left\|u_h^0\right\|^2 + 2|\Omega| \leq C_0 + 2|\Omega|.
\end{aligned} \tag{4.15}$$

By definition, $\left\| \frac{u_h^{n+1} - u_h^n}{\tau} \right\|_{-1,h} = \left\|\nabla \tilde{w}_h^{n+1}\right\|$, and the energy stability reads

$$\mathcal{E}(u_h^{n+1}, u_h^n) + \tau \cdot \kappa_A \left\|\nabla \tilde{w}_h^{n+1}\right\|^2 \leq \mathcal{E}(u_h^n, u_h^{n-1}), \quad n \geq 1.$$

Therefore, for any $m \geq 2$,

$$E(u_h^m) \leq \mathcal{E}(u_h^m, u_h^{m-1}) + \tau \cdot \kappa_A \sum_{n=2}^{m} \|\nabla \tilde{w}_h^n\|^2 \leq \mathcal{E}(u_h^1, u_h^0) \leq C_0 + 2|\Omega|. \tag{4.16}$$

It follows that, for any $m \geq 0$

$$\|u_h^m\|_{H^1}^2 \leq \frac{2(C_0 + 3|\Omega|)}{\varepsilon^2} =: C_1,$$

assuming that $\varepsilon \leq 1$. Next, using the stability (4.9) and the fact that $\nabla \tilde{w}_h^1 = \nabla w_h^1$, we have, for any $m \geq 1$,

$$\tau \cdot \kappa_A \sum_{n=1}^{m} \left\| \frac{u_h^n - u_h^{n-1}}{\tau} \right\|_{-1,h}^2 = \tau \cdot \kappa_A \sum_{n=1}^{m} \|\nabla \tilde{w}_h^n\|^2 \leq \frac{4C_0}{3} + 2|\Omega| =: C_2.$$

Finally, for some time varying mass parameter $\alpha^n \in \mathbb{R}$,

$$w_h^n = \alpha^n + \begin{cases} \frac{3}{2}\tilde{w}_h^n - \frac{1}{2}\tilde{w}_h^{n-1}, & n \geq 2 \\ \tilde{w}_h^1, & n = 1, \end{cases}$$

which implies that $\|\nabla w_h^n\| \leq 2\|\nabla \tilde{w}_h^n\|$. We can conclude that

$$\tau \cdot \kappa_A \sum_{n=1}^{m} \|\nabla w_h^n\|^2 \leq 4C_2 =: C_3,$$

and the proof is complete. ∎

5. Convergence analysis and error estimate. We denote the exact solution as $u^n = u(\mathbf{x}, t^n)$ at $t = t^n$. As usual, a regularity assumption has to be made in the error analysis, and we denote all the upper bounds for the exact solution as C_0. The following estimates hold for Ritz projection [6]:

$$\|R_h\varphi\|_{1,p} \le C\|\varphi\|_{1,p}, \qquad \forall 1 < p \le \infty, \tag{5.1}$$

$$\|\varphi - R_h\varphi\|_p + h\|\varphi - R_h\varphi\|_{1,p} \le Ch^{q+1}\|\varphi\|_{q+1,p}, \qquad \forall 1 < p \le \infty. \tag{5.2}$$

Suppose that $u \in L^\infty(0,T;W^{1,p})$. Combining (5.1) and the Sobolev imbedding theorem: $W^{1,p}(\Omega) \hookrightarrow L^\infty(\Omega)$, for $2 < p \le \infty$ ($d = 2$), $3 < p \le \infty$ ($d = 3$), there are constants $C_4, C_5 > 0$ such that

$$\|u^n\|_\infty \le C\|u^n\|_{1,p} \le C_4,$$
$$\|R_h u^n\|_\infty \le C\|R_h u^n\|_{1,p} \le C\|u^n\|_{1,p} \le C_5.$$

The following discrete Gronwall inequality is needed in the error analysis.

LEMMA 5.1. *For a fixed $T = \tau \cdot N$, where N is a positive integer, and $\tau > 0$, assume that $\{a^n\}_{n=1}^N, \{b^n\}_{n=1}^N$ and $\{c^n\}_{n=1}^{N-1}$ are all non-negative sequences, with $\tau\sum_{n=1}^{N-1} c^n \le C_6$, where $C_6 > 0$ is independent of τ and N, but possibly dependent on T. If for all $\tau > 0$, there is some $C_7 > 0$, which is independent of τ and N, such that*

$$a^N + \tau\sum_{n=1}^{N} b^n \le C_7 + \tau\sum_{n=1}^{N-1} a^n c^n,$$

then

$$a^N + \tau\sum_{n=1}^{N} b^n \le (C_7 + \tau a^0 c^0)\exp\left(\tau\sum_{n=1}^{N-1} c^n\right) \le (C_7 + \tau a^0 c^0)\exp(C_6).$$

Before proceeding into the convergence analysis, we introduce a new norm. Let Ω be an arbitrary bounded domain and $\mathbf{p} = [u, v]^T \in \left[L^2(\Omega)\right]^2$. We define the G-norm to be a weighted inner product

$$\|\mathbf{p}\|_{\mathsf{G}}^2 = (\mathbf{p}, \mathsf{G}\mathbf{p}), \quad \mathsf{G} = \begin{bmatrix} \frac{1}{2} & -1 \\ -1 & \frac{5}{2} \end{bmatrix}.$$

Since G is symmetric positive definite, the norm is well-defined. Moreover,

$$\mathsf{G} = \begin{bmatrix} \frac{1}{2} & -1 \\ -1 & \frac{5}{2} \end{bmatrix} = \begin{bmatrix} \frac{1}{2} & -1 \\ -1 & 2 \end{bmatrix} + \begin{bmatrix} 0 & 0 \\ 0 & \frac{1}{2} \end{bmatrix} =: \mathsf{G}_1 + \mathsf{G}_2,$$

By the positive semi-definiteness of G_1, we immediately have

$$\|\mathbf{p}\|_{\mathsf{G}}^2 = (\mathbf{p}, (\mathsf{G}_1 + \mathsf{G}_2)\mathbf{p}) \ge (\mathbf{p}, \mathsf{G}_2\mathbf{p}) = \frac{1}{2}\|v\|^2. \tag{5.3}$$

In addition, for any $v_i \in L^2(\Omega), i = 0, 1, 2$, the following equality is valid:

$$\left(\frac{3}{2}v_2 - 2v_1 + \frac{1}{2}v_0, v_2\right) = \frac{1}{2}(\|\mathbf{p}_2\|_{\mathsf{G}}^2 - \|\mathbf{p}_1\|_{\mathsf{G}}^2) + \frac{\|v_2 - 2v_1 + v_0\|^2}{4}, \tag{5.4}$$

with $\mathbf{p}_1 = [v_0, v_1]^T, \mathbf{p}_2 = [v_1, v_2]^T$.

By (u, w) we denote the exact solution to the original CH equation (1.2). We say that the solution pair of regularity of class $\mathcal{C}$ if and only if

$$u \in W^{3,\infty}(0,T;L^2) \cap W^{1,\infty}(0,T;H^{q+1}), \tag{5.5}$$

$$w \in L^2(0,T;H^{q+1}). \tag{5.6}$$

The following theorem is the main result of this section.

THEOREM 5.1. *Suppose that the exact solution pair (u, w) is in the regularity class $\mathcal{C}$, for the fixed final time $T > 0$. Let $u^n = u(t^n)$ and u_h^n be the solution at time $t = t^n$ to the fully discrete numerical scheme (2.2), for $1 \le n \le N$, with $N \cdot \tau = T$. Then we have the error estimate*

$$\|u^n - u_h^n\| + \left(\tau\varepsilon^2 \sum_{k=1}^{n} \|\Delta_h(R_h u^k - u_h^k)\|^2 \right)^{1/2} \le C_8(h^{q+1} + \tau^2), \tag{5.7}$$

for some constant $C_8 > 0$ that is independent of τ and h.

Proof. First we define error functions: $e_u^n := u^n - u_h^n$, $e_w^n := w^n - w_h^n$. Then the following equations for the error functions hold: for any $v_h, \psi_h \in S_h$,

$$\left(\delta_\tau e_u^{n+1}, v_h\right) + (\nabla e_w^{n+1}, \nabla v_h) = -\left(\mathcal{R}_1^{n+1}, v_h\right), \tag{5.8}$$

$$\begin{aligned}\varepsilon^2(\nabla e_u^{n+1}, \nabla\psi_h) - (e_w^{n+1}, \psi_h) + \tau(\nabla T_2^{n+1}, \nabla\psi_h) &= (T_1^{n+1} - T_3^{n+1}, \psi_h) \\ &\quad + (\mathcal{R}_2^{n+1} - \mathcal{R}_3^{n+1}, \psi_h),\end{aligned} \tag{5.9}$$

where

$$\delta_\tau v^{n+1} := \begin{cases} \frac{3v^{n+1} - 4v^n + v^{n-1}}{2\tau}, & n \ge 1 \\ \frac{v^1 - v^0}{\tau}, & n = 0 \end{cases}, \tag{5.10}$$

$$\mathcal{R}_1^{n+1} := u_t^{n+1} - \delta_\tau u^{n+1}, \tag{5.11}$$

$$\mathcal{R}_2^{n+1} := u^{n+1} - \begin{cases} 2u^n - u^{n-1}, & n \ge 1 \\ u^0, & n = 0 \end{cases}, \tag{5.12}$$

$$\mathcal{R}_3^{n+1} := \begin{cases} A\tau\Delta(u^{n+1} - u^n), & n \ge 1 \\ 0, & n = 0 \end{cases}, \tag{5.13}$$

$$T_1^{n+1} := \begin{cases} 2e_u^n - e_u^{n-1}, & n \ge 1 \\ e_u^0, & n = 0 \end{cases}, \tag{5.14}$$

$$T_2^{n+1} := \begin{cases} A(e_u^{n+1} - e_u^n), & n \ge 1 \\ 0, & n = 0 \end{cases}, \tag{5.15}$$

$$T_3^{n+1} := (u^{n+1})^3 - (u_h^{n+1})^3. \tag{5.16}$$

By the Cauchy-Schwarz inequality, we have the following estimate

$$\begin{aligned}\|\mathcal{R}_1^{n+1}\|^2 &\le \begin{cases} 32\tau^3 \int_{t_{n-1}}^{t_{n+1}} \|\partial_{ttt} u\|^2 dt, & n \ge 1 \\ \frac{\tau}{3} \int_0^{t_1} \|\partial_{tt} u\|^2 dt, & n = 0 \end{cases} \\ &\le \begin{cases} 32\tau^3 \int_{t_{n-1}}^{t_{n+1}} \|\partial_{ttt} u\|^2 dt, & n \ge 1 \\ \frac{\tau^2}{3} \|u\|_{W^{2,\infty}(0,T;L^2)}, & n = 0 \end{cases} \\ &\le \begin{cases} 32\tau^3 \int_{t_{n-1}}^{t_{n+1}} \|\partial_{ttt} u\|^2 dt, & n \ge 1 \\ C_9\tau^2, & n = 0 \end{cases}. \end{aligned} \tag{5.17}$$

An analogous estimate is available for the second remainder term: for the case $n \geq 1$, we have

$$\|\mathcal{R}_2^{n+1}\|^2 \leq 32\tau^3 \int_{t_{n-1}}^{t_{n+1}} \|\partial_{tt} u\|^2 dt.$$

We will not directly need an estimate of $\left\|\mathcal{R}_2^1\right\|$, but we will address the control of $\mathcal{R}_2^1$ shortly. For the third remainder term, we obtain the estimate

$$\|\mathcal{R}_3^{n+1}\|^2 \leq \begin{cases} A^2\tau^3 \int_{t_n}^{t_{n+1}} \|\partial_t \Delta u\|^2 dt, & n \geq 1 \\ 0, & n = 0 \end{cases}.$$

Suppose $v_h \in S_h$ is arbitrary. Using the definitions of Ritz projection and the discrete Laplacian, Δ_h, we have

$$\begin{aligned}
(\nabla e_w^{n+1}, \nabla v_h) &= (\nabla w^{n+1} - \nabla R_h w^{n+1}, \nabla v_h) + (\nabla R_h w^{n+1} - \nabla w_h^{n+1}, \nabla v_h) \\
&= (\nabla (R_h w^{n+1} - w_h^{n+1}), \nabla v_h) \\
&= (R_h w^{n+1} - w_h^{n+1}, -\Delta_h v_h) \\
&= (w^{n+1} - w_h^{n+1} + R_h w^{n+1} - w^{n+1}, -\Delta_h v_h) \\
&= (e_w^{n+1}, -\Delta_h v_h) - (w^{n+1} - R_h w^{n+1}, -\Delta_h v_h).
\end{aligned}$$

Combining the last equation with the error equations (5.9) and (5.8), and taking $\psi_h = -\Delta_h v_h$, yields

$$\begin{aligned}
\left(\delta_\tau e_u^{n+1}, v_h\right) &+ \tau(\nabla T_2^{n+1}, \nabla(-\Delta_h) v_h) + \varepsilon^2 (\nabla e_u^{n+1}, \nabla(-\Delta_h) v_h) \\
&= -(\mathcal{R}_1^{n+1}, v_h) + (T_1^{n+1} - T_3^{n+1}, -\Delta_h v_h) \\
&\quad + (\mathcal{R}_2^{n+1} - \mathcal{R}_3^{n+1}, -\Delta_h v_h) + (w^{n+1} - R_h w^{n+1}, -\Delta_h v_h).
\end{aligned}$$

Denote $\rho^{n+1} := u^{n+1} - R_h u^{n+1}$ and $\sigma_h^{n+1} := R_h u^{n+1} - u_h^{n+1}$, then we get $e_u^{n+1} = \rho^{n+1} + \sigma_h^{n+1}$. By the definition (2.3) of Ritz projection, it holds that $(\nabla \rho^{n+1}, \nabla \chi) = 0$, for all $\chi \in S_h$. Therefore, with $v_h = \sigma_h^{n+1}$, the error equation can be written as follows:

$$\begin{aligned}
\left(\delta_\tau \sigma_h^{n+1}, \sigma_h^{n+1}\right) &+ \epsilon^2 \|\Delta_h \sigma_h^{n+1}\|^2 + \tau(\nabla T_{2,h}^{n+1}, \nabla(-\Delta_h)\sigma_h^{n+1}) \\
&= -(\mathcal{R}_1^{n+1}, \sigma_h^{n+1}) - (T_3^{n+1}, -\Delta_h \sigma_h^{n+1}) + (T_{1,a}^{n+1}, -\Delta_h \sigma_h^{n+1}) \\
&\quad + (T_{1,h}^{n+1}, -\Delta_h \sigma_h^{n+1}) + (\mathcal{R}_2^{n+1}, -\Delta_h \sigma_h^{n+1}) - (\mathcal{R}_3^{n+1}, -\Delta_h \sigma_h^{n+1}) \\
&\quad + (w^{n+1} - R_h w^{n+1}, -\Delta_h \sigma_h^{n+1}) - (\delta_\tau \rho^{n+1}, \sigma_h^{n+1}) \\
&=: J_1 + J_2 + J_3 + J_4 + J_5 + J_6 + J_7 + J_8 =: J,
\end{aligned} \tag{5.18}$$

where

$$T_{1,a}^{n+1} := \begin{cases} 2\rho^n - \rho^{n-1}, & n \geq 1 \\ \rho^0, & n = 0 \end{cases}, \tag{5.19}$$

$$T_{1,h}^{n+1} := \begin{cases} 2\sigma_h^n - \sigma_h^{n-1}, & n \geq 1 \\ \sigma_h^0 \equiv 0, & n = 0 \end{cases}, \tag{5.20}$$

$$T_{2,h}^{n+1} := \begin{cases} A(\sigma_h^{n+1} - \sigma_h^n), & n \geq 1 \\ 0, & n = 0 \end{cases}. \tag{5.21}$$

Observe that $\sigma_h^0 \equiv 0$, because of our choice of initial data.

Now look at the left-hand side of (5.18). From (5.4), we have

$$\left(\delta_\tau \sigma_h^{n+1}, \sigma_h^{n+1}\right) = \begin{cases} \frac{1}{2\tau}(\|\mathbf{p}^{n+1}\|_{\mathsf{G}}^2 - \|\mathbf{p}^n\|_{\mathsf{G}}^2) + \frac{1}{4\tau}\|\sigma_h^{n+1} - 2\sigma_h^n + \sigma_h^{n-1}\|^2, & n \geq 1 \\ \frac{1}{2\tau}(\|\sigma_h^1\|^2 - \|\sigma_h^0\|^2) + \frac{1}{2\tau}\|\sigma_h^1 - \sigma_h^0\|^2, & n = 0 \end{cases}, \tag{5.22}$$

where $\mathbf{p}^{k+1} = [\sigma_h^k, \sigma_h^{k+1}]^T$. Using the definition of Δ_h, it follows that

$$\begin{aligned} \tau(\nabla T_{2,h}^{n+1}, \nabla(-\Delta_h)\sigma_h^{n+1}) &= A\tau(-\Delta_h \sigma_h^{n+1} + \Delta_h \sigma_h^n, -\Delta_h \sigma_h^{n+1}) \\ &\geq \frac{1}{2} A\tau(\|\Delta_h \sigma_h^{n+1}\|^2 - \|\Delta_h \sigma_h^n\|^2). \end{aligned}$$

As a result, the left-hand side of (5.18) is bounded from below: for $n \geq 1$,

$$\frac{1}{2\tau}\left(\|\mathbf{p}^{n+1}\|_{\mathsf{G}}^2 - \|\mathbf{p}^n\|_{\mathsf{G}}^2\right) + \frac{1}{2} A\tau\left(\|\Delta_h \sigma_h^{n+1}\|^2 - \|\Delta_h \sigma_h^n\|^2\right) + \epsilon^2 \|\Delta_h \sigma_h^{n+1}\|^2 \leq J,$$

and, for $n = 0$,

$$\frac{1}{2\tau}\|\sigma_h^1\|^2 + \epsilon^2 \|\Delta_h \sigma_h^1\|^2 \leq J.$$

Now we study the seven terms on the right-hand side of (5.18).

$$\begin{aligned} J_1 = (-\mathcal{R}_1^{n+1}, \sigma_h^{n+1}) &\leq \|\mathcal{R}_1^{n+1}\| \cdot \|\sigma_h^{n+1}\| \\ &\leq \begin{cases} 32\tau^3 \int_{t_{n-1}}^{t_{n+1}} \|\partial_{ttt} u\|^2 dt + \frac{1}{4}\|\sigma_h^{n+1}\|^2, & n \geq 1 \\ 2C_9 \tau^3 + \frac{1}{8\tau}\|\sigma_h^1\|^2, & n = 0 \end{cases}. \end{aligned}$$

For J_8, we have

$$J_8 = -\left(\delta_\tau \rho^{n+1}, \sigma_h^{n+1}\right) \leq \left\|\delta_\tau \rho^{n+1}\right\|^2 + \frac{1}{4}\|\sigma_h^{n+1}\|^2.$$

In addition, (5.2) indicates that

$$\begin{aligned} \left\|\delta_\tau \rho^{n+1}\right\|^2 = \ & \left\|(I - R_h)\delta_\tau u^{n+1}\right\|^2 \\ &\leq \begin{cases} \frac{9Ch^{2(q+1)}}{2\tau} \int_{t_{n-1}}^{t_{n+1}} \|\partial_t u\|_{H^{q+1}}^2 dt, & n \geq 1 \\ \frac{Ch^{2(q+1)}}{\tau} \int_0^{t_1} \|\partial_t u\|_{H^{q+1}}^2 \, dt, & n = 0 \end{cases}, \end{aligned}$$

which, in turn, shows that, for all $0 \leq n \leq N-1$,

$$J_8 \leq \begin{cases} \frac{9Ch^{2(q+1)}}{2\tau} \int_{t_{n-1}}^{t_{n+1}} \|\partial_t u\|_{H^{q+1}}^2 dt + \frac{1}{4}\|\sigma_h^{n+1}\|^2, & n \geq 1 \\ \frac{Ch^{2(q+1)}}{\tau} \int_0^{t_1} \|\partial_t u\|_{H^{q+1}}^2 dt + \frac{1}{4}\|\sigma_h^1\|^2, & n = 0 \end{cases}.$$

For J_5, we estimate the $n = 0$ and $n \geq 1$ cases separately. For $n \geq 1$,

$$J_5 = (\mathcal{R}_2^{n+1}, -\Delta_h \sigma_h^{n+1}) \leq \frac{4}{\varepsilon^2} 32\tau^3 \int_{t_{n-1}}^{t_{n+1}} \|\partial_{tt} u\|^2 dt + \frac{\varepsilon^2}{16}\|\Delta_h \sigma_h^{n+1}\|^2. \tag{5.23}$$

To facilitate the special analysis for the initialization step, we need a more careful approach. For $n = 0$, we proceed as follows: using the definition of the Ritz projection,

the discrete Laplacian, and the stability (3.1),

$$\begin{aligned} J_5 &= (\mathcal{R}_2^1, -\Delta_h \sigma_h^1) = (\rho^1 - \rho^0, -\Delta_h \sigma_h^1) + (R_h(u^1 - u^0), -\Delta_h \sigma_h^1) \\ &= (\rho^1 - \rho^0, -\Delta_h \sigma_h^1) - (\Delta_h(R_h(u^1 - u^0)), \sigma_h^1) \\ &\le \left\|\rho^1 - \rho^0\right\| \cdot \left\|\Delta_h \sigma_h^1\right\| + \left\|\Delta_h(R_h(u^1 - u^0))\right\| \cdot \left\|\sigma_h^1\right\| \\ &\le \left\|\rho^1 - \rho^0\right\| \cdot \left\|\Delta_h \sigma_h^1\right\| + \left\|\Delta(u^1 - u^0)\right\| \cdot \left\|\sigma_h^1\right\| \\ &\le \frac{2}{\varepsilon^2} \frac{C h^{2(q+1)}}{\tau} \int_0^{t_1} \|\partial_t u\|_{H^{q+1}}^2 dt + \frac{\varepsilon^2}{8} \|\Delta_h \sigma_h^1\|^2 \\ &\quad + 2C_{10}\tau^3 + \frac{1}{8\tau} \|\sigma_h^1\|^2. \end{aligned} \tag{5.24}$$

Here we have made use of the estimate

$$\left\|\Delta(u^1 - u^0)\right\|^2 \le \tau \int_0^{t_1} \left\|\partial_t \Delta u\right\|^2 dt \le \tau^2 \left\|u\right\|_{W^{1,\infty}(0,T;H^2)} \le C_{10}\tau^2.$$

For J_6, we have

$$\begin{aligned} J_6 &\le \|\mathcal{R}_3^{n+1}\| \cdot \|\Delta_h \sigma_h^{n+1}\|^2 \\ &\le \begin{cases} \frac{4}{\varepsilon^2} A^2 \tau^3 \int_{t_n}^{t_{n+1}} \|\partial_t \Delta u\|^2 dt + \frac{\varepsilon^2}{16} \|\Delta_h \sigma_h^{n+1}\|^2, & n \ge 1 \\ 0, & n = 0 \end{cases}. \end{aligned} \tag{5.25}$$

For J_7 and J_3, we have, using the standard finite element approximations,

$$J_7 = ((I - R_h) w^{n+1}, -\Delta_h \sigma_h^{n+1}) \le \frac{2Ch^{2(q+1)}}{\varepsilon^2} \|w^{n+1}\|_{H^{q+1}}^2 + \frac{\varepsilon^2}{8} \|\Delta_h \sigma_h^{n+1}\|^2, \tag{5.26}$$

and

$$\begin{aligned} J_3 &= (T_{1,a}^{n+1}, -\Delta_h \sigma_h^{n+1}) \le \frac{2}{\varepsilon^2} \|T_{1,a}^{n+1}\|^2 + \frac{\varepsilon^2}{8} \|\Delta_h \sigma_h^{n+1}\|^2 \\ &\le \frac{\varepsilon^2}{8} \|\Delta_h \sigma_h^{n+1}\|^2 + \frac{4Ch^{2(q+1)}}{\varepsilon^2} \begin{cases} 4\|u^n\|_{H^{q+1}}^2 + \|u^{n-1}\|_{H^{q+1}}^2, & n \ge 1 \\ \|u^0\|_{H^{q+1}}^2, & n = 0 \end{cases}. \end{aligned} \tag{5.27}$$

For J_4,

$$J_4 = (T_{1,h}^{n+1}, -\Delta_h \sigma_h^{n+1}) \le \frac{2}{\varepsilon^2} \|T_{1,h}^{n+1}\|^2 + \frac{\varepsilon^2}{8} \|\Delta_h \sigma_h^{n+1}\|^2 \tag{5.28}$$

$$\le \frac{\varepsilon^2}{8} \|\Delta_h \sigma_h^{n+1}\|^2 + \frac{4}{\varepsilon^2} \begin{cases} 4\|\sigma_h^n\|^2 + \|\sigma_h^{n-1}\|^2, & n \ge 1 \\ 0, & n = 0 \end{cases}. \tag{5.29}$$

The analysis of the nonlinear term is given by (5.33) in Proposition 5.1:

$$J_2 \le \frac{2C_{11}h^{2(q+1)}}{\varepsilon^2} \|u^{n+1}\|_{H^{q+1}}^2 + \frac{54}{\varepsilon^6} C_{12}^4 \|\sigma_h^{n+1}\|^2 + \frac{\varepsilon^2}{4} \|\Delta_h \sigma_h^{n+1}\|^2.$$

Substituting these terms into (5.18), and multiplying by 2τ on both sides, we have,

for $n \geq 1$,

$$\begin{aligned}
&\|\mathbf{p}^{n+1}\|_{\mathsf{G}}^2 - \|\mathbf{p}^n\|_{\mathsf{G}}^2 + A\tau^2(\|\Delta_h\sigma_h^{n+1}\|^2 - \|\Delta_h\sigma_h^n\|^2) + \frac{\tau\varepsilon^2}{2}\|\Delta_h\sigma_h^{n+1}\|^2 \\
&\quad \leq \left(1 + \frac{108}{\varepsilon^6}C_{12}^4\right)\tau\|\sigma_h^{n+1}\|^2 + \frac{32\tau}{\varepsilon^2}\|\sigma_h^n\|^2 + \frac{8\tau}{\varepsilon^2}\|\sigma_h^{n-1}\|^2 \\
&\qquad + 9Ch^{2(q+1)}\int_{t_{n-1}}^{t_{n+1}}\|\partial_t u\|_{H^{q+1}}^2 dt + \frac{4Ch^{2(q+1)}}{\varepsilon^2}\tau\|w^{n+1}\|_{H^{q+1}}^2 \\
&\qquad + \frac{4}{\varepsilon^2}C_{11}\tau h^{2(q+1)}\|u^{n+1}\|_{H^{q+1}}^2 + \frac{32C}{\varepsilon^2}\tau h^{2(q+1)}\|u^n\|_{H^{q+1}}^2 \\
&\qquad + \frac{8C}{\varepsilon^2}\tau h^{2(q+1)}\|u^{n-1}\|_{H^{q+1}}^2 + 64\tau^4\int_{t_{n-1}}^{t_{n+1}}\|\partial_{ttt}u\|^2 dt \\
&\qquad + \frac{8}{\varepsilon^2}\tau^4\left(32\int_{t_{n-1}}^{t_{n+1}}\|\partial_{tt}u\|^2 dt + A^2\int_{t_n}^{t_{n+1}}\|\partial_t\Delta u\|^2 dt\right).
\end{aligned} \tag{5.30}$$

For $n = 0$, we have a similar form:

$$\begin{aligned}
&\|\sigma_h^1\|^2 + 2\tau\varepsilon^2\|\Delta_h\sigma_h^1\|^2 \\
&\quad \leq \left(\frac{\tau}{2} + \frac{1}{2} + \frac{108\tau}{\varepsilon^6}C_{12}^4\right)\|\sigma_h^1\|^2 + \frac{3\tau\varepsilon^2}{2}\|\Delta_h\sigma_h^1\|^2 + 2Ch^{2(q+1)}\int_0^{t_1}\|\partial_t u\|_{H^{q+1}}^2 dt \\
&\qquad + \frac{4Ch^{2(q+1)}}{\varepsilon^2}\tau\|w^1\|_{H^{q+1}}^2 + \frac{4}{\varepsilon^2}C_{11}\tau h^{2(q+1)}\|u^1\|_{H^{q+1}}^2 \\
&\qquad + \frac{8C}{\varepsilon^2}\tau h^{2(q+1)}\|u^0\|_{H^{q+1}}^2 + \frac{4}{\varepsilon^2}Ch^{2(q+1)}\int_0^{t_1}\|\partial_t u\|_{H^{q+1}}^2 dt + 4\tau^4 C_9 + 4\tau^4 C_{10}.
\end{aligned} \tag{5.31}$$

With the help of Proposition 5.2, we get

$$\|\sigma_h^{n+1}\| + \left(\tau\varepsilon^2\sum_{k=1}^{n+1}\|\Delta_h\sigma_h^k\|^2\right)^{1/2} \leq C_{T,\varepsilon}(h^{q+1} + \tau^2), \tag{5.32}$$

with $C_{T,\varepsilon}$ independent of τ and h. In addition, it is easy to see from (5.2) that

$$\|\rho^k\| \leq Ch^{q+1}\|u^k\|_{H^{q+1}}, \quad 1 \leq k \leq n+1.$$

Together with the triangle inequality $\|e_u^{n+1}\| \leq \|\rho^{n+1}\| + \|\sigma_h^{n+1}\|$, we finally arrive at the conclusion of the theorem. □

The following two propositions are used in the convergence analysis; their proofs are given in the Appendix.

PROPOSITION 5.1. *For the nonlinear error inner product term J_2, as given by* (5.18)*, we have*

$$J_2 \leq \frac{2C_{11}h^{2(q+1)}}{\varepsilon^2}\|u^{n+1}\|_{H^{q+1}}^2 + \frac{54}{\varepsilon^6}C_{12}^4\|\sigma_h^{n+1}\|^2 + \frac{\varepsilon^2}{4}\|\Delta_h\sigma_h^{n+1}\|^2. \tag{5.33}$$

PROPOSITION 5.2. *By the error evolution inequalities* (5.30), (5.31)*, the following convergence estimate is valid:*

$$\|\sigma_h^{n+1}\| + \left(\tau\varepsilon^2\sum_{k=1}^{n+1}\|\Delta_h\sigma_h^k\|^2\right)^{1/2} \leq C_{T,\varepsilon}(h^{q+1} + \tau^2), \tag{5.34}$$

with $C_{T,\varepsilon}$ independent of τ and h, under a technical assumption

$$0 < \tau \le \frac{1}{4}\left(1 + \frac{108}{\varepsilon^6} C_{12}^4\right)^{-1} := \tau_1. \tag{5.35}$$

REMARK 5.1. *We note that the $\ell^\infty(0,T;L^2) \cap \ell^2(0,T;H_h^2)$ convergence (5.7) is unconditional in the following sense: there is no restriction for τ in terms of h to guarantee convergence. In fact, the energy stability estimate (given by Theorem 4.1) plays an essential role in the derivation of this unconditional convergence analysis. Specifically, the uniform-in-time H^1 estimate (4.12), a direct consequence of (4.2), leads to an $\ell^\infty(0,T;L^6)$ bound of the numerical solution. As a result, the nonlinear coefficients are bounded in the estimate (A.2), and we only need to handle the L^6 and discrete H^2 norms of the projection error function. This could be accomplished via repeated applications of 3-D Sobolev inequalities. Finally, an unconditional convergence estimate becomes available.*

REMARK 5.2. *It is observed that, the time step requirement* (5.35)*, which states that $\tau \le C\varepsilon^6$, may be very restrictive. On the other hand, this requirement is only associated with a theoretical justification of the $\ell^\infty(0,T;L^2)$ convergence analysis, and such a restriction is not needed in the practical computations. In fact, if we pursue an $\ell^\infty(0,T;H^{-1})$ error estimate, no time step requirement is needed, due to the following inequality:*

$$\begin{aligned}&((R_h u^{n+1})^3 - (u_h^{n+1})^3, \sigma_h^{n+1}) \\ &\quad = ((R_h u^{n+1})^2 + R_h u^{n+1} u_h^{n+1} + (u_h^{n+1})^2, (\sigma_h^{n+1})^2) \ge 0,\end{aligned} \tag{5.36}$$

so that the nonlinear error inner product becomes trivial; also see the related discussion in [19]. In addition, for the two-dimensional CH flow, this restriction could be reduced to $\tau \le C\varepsilon^{2+\delta}$, even for the $\ell^\infty(0,T;L^2)$ error estimate, since the H^1 bound of the numerical solution ensures an embedding into the L^q norm, for any $q > 2$.

In more detail, due to an implicit treatment of the nonlinear term in the proposed numerical scheme, the time step requirement (5.35) *is needed to pass through the discrete Gronwall inequality. Instead, for the epitaxial thin film growth without slope selection, such a restriction could be reduced to $\tau \le C\varepsilon^2$, due to the crucial fact that the higher order derivative of the nonlinear term has an automatic L^∞ bound; see the detailed convergence analyses in recent articles [10, 29].*

6. Numerical results.

6.1. Accuracy check and convergence test. In this subsection we apply the fully discrete second order BDF scheme (2.2) to perform a numerical accuracy check. In a two-dimensional computational domain $\Omega = (0,1)^2$, and the exact solution for the phase variable is given by

$$u_e(x,y,t) = \cos(\pi x)\cos(\pi y)\mathrm{e}^{-t}. \tag{6.1}$$

In turn, u_e satisfies the original PDE (1.2), with an artificial, time-dependent forcing term added on the right hand side:

$$\partial_t u_e = \Delta(u_e^3 - u_e - \varepsilon^2 \Delta u_e) + g, \qquad (x,y,t) \in \Omega \times (0,T]. \tag{6.2}$$

The final time is taken to be $T = 1$, and the physical parameter is given by $\varepsilon^2 = 0.05$.

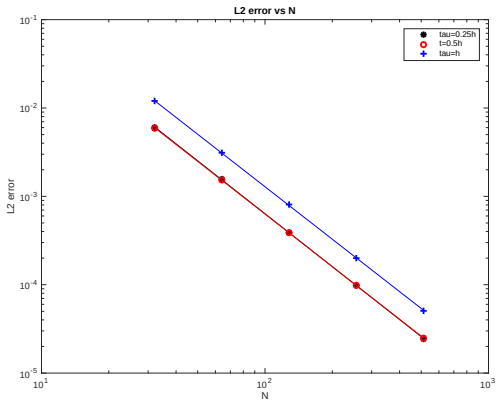

FIG. 6.1. *L^2 numerical errors at $T = 1.0$ plotted versus N for the second order BDF scheme (2.2). The surface diffusion parameter is taken to be $\varepsilon^2 = 0.05$ and the time step size is given by $\tau = 0.25h$, $\tau = 0.5h$, $\tau = h$, respectively. The data lie roughly on curves CN^{-2}, for appropriate choices of C, confirming the full second-order accuracy of the scheme.*

The nonlinear equations are solved by Newton's method. In the iteration process, the initial guess is chosen to be a second order extrapolation of the previous two steps, i.e., $u_h^{n+1,0} = 2u_h^n - u_h^{n-1}$, which usually leads to one iteration stage less than the one with an initial guess as $u_h^{n+1,0} = u_h^n$. Therefore, this methodology reduces the computation cost. The stopping criterion for the nonlinear iteration is given by $\|u_h^{n+1,(m)} - u_h^{n+1,(m-1)}\| < \delta^3$, with $\delta = h$.

We compute solutions with grid sizes $N = 32, 64, 128, 256, 512$, with the L^2 errors reported at the final time $T = 1$. The time step is determined by a few different linear refinement paths: $\tau = 0.25h$, $\tau = 0.5h$, and $\tau = h$, respectively, where h is the spatial grid size. Figure 6.1 shows the L^2 error between the numerical and exact solutions. A clear second order accuracy, for both the temporal and spatial approximations, is observed in the convergence test. We also note that, the convergence constant associated with $\tau = 0.25h$ is almost the same as the one associated with $\tau = 0.5h$. This interesting phenomenon is associated with the following subtle fact: the temporal truncation error is associated with the fourth order temporal derivative, while the spatial truncation error is associated with the sixth order spatial derivatives. Meanwhile, for the exact test function (6.1), the fourth order temporal derivative is in a much smaller numerical scale than the sixth order spatial derivatives. In turn, the overall numerical error is dominated by the spatial ones; with a decreasing values of time step size, the temporal errors will become more and more negligible. Therefore, the difference of convergence constants could be clearly observed between $\tau = h$ and $\tau = 0.5h$, while the overall convergence constants for $\tau = 0.5h$ and $\tau = 0.25h$ are almost the same in the figure.

In addition, to test whether a larger value of A may lead to a bigger numerical error, we perform the numerical accuracy check with a sequence of A: $A = 0$, $\frac{1}{16}$, 1, 2 and 4, and report the corresponding numerical errors, defined as the difference between the numerical solutions and the exact test function (6.1), in Figure 6.2. It is observed that, a bigger value of A may give less accurate solutions when $A \geq 1$; while for $A < 1$, numerical errors are at a comparable level. In particular, the right part of Figure 6.2 shows the L^2 errors for different choices of A for $N = 64$.

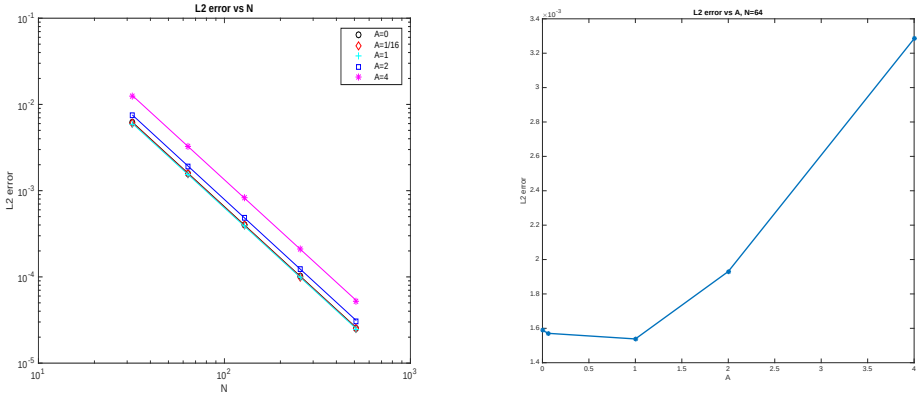

FIG. 6.2. *Left: L^2 numerical errors at $T = 1.0$ plotted versus N, with the same physical parameter as Figure 6.1, the time step size $\tau = 0.5h$, and different values of A. Right: L^2 error versus A, with $N = 64$.*

Another interesting phenomenon to be observed in Figure 6.2 is that, the numerical scheme with $A = 1$ yields the smallest numerical error, instead of the one with $A = 0$. Such a performance comes from the following subtle fact: the artificial Douglas-Dupont regularization term, $-A\tau\Delta^2(u^{k+1} - u^k)$, leads to an $O(\tau^2)$ local truncation error. In turn, its combination with the truncation error associated with the 2nd order BDF stencil approximation gives the overall temporal truncation error. More interestingly, these two truncation errors have the maximum cancellation effect with $A = 1$; that is the reason why the L^2 numerical error associated with $A = 1$ is even better than the one with $A = 0$. On the other hand, with an increasing value of A, such a cancellation effect vanishes; that is the reason why the L^2 numerical error with $A = 2$ and $A = 4$ become larger than the ones with $A \leq 1$.

6.2. Numerical simulation of coarsening process. A numerical simulation result of a physics example is presented in this subsection. In particular, the long time evolution scaling law for certain physical quantities, such as the energy, has caused a great deal of scientific interests, with the assumption that the interface width is in a much smaller scale than the domain size, i.e., $\varepsilon \ll \min\{L_x, L_y\}$, with $\Omega = (0, L_x) \times (0, L_y)$. A formal analysis has indicated a lower decay bound as $t^{-1/3}$ for the energy dissipation law, with the lower bound typically observed for the averaged values of the energy quantity. A numerical prediction of this scaling law turns out to be a challenging work, due to the fact that both short and long-time accuracy and stability are required in the large time scale simulation, in particular for small values of ε.

We compare the numerical simulation result with the predicted coarsening rate, using the proposed second order BDF scheme (2.2) for the Cahn-Hilliard flow (1.2). The surface diffusion coefficient parameter is taken to be $\varepsilon^2 = 0.005$, and the computational domain is taken to be $\Omega = (0, 12.8)^2$. For the spatial discretization, we use a resolution of $N = 256$, which is sufficient to resolve the small structures for such a value of ε.

For the temporal step size, we use increasing values of τ in the time evolution. In more detail, $\tau = 0.004$ on the time interval $[0, 100]$, $\tau = 0.04$ on the time interval $[100, 2000]$. Whenever a new time step size is applied, we initiate the two-step numeri-

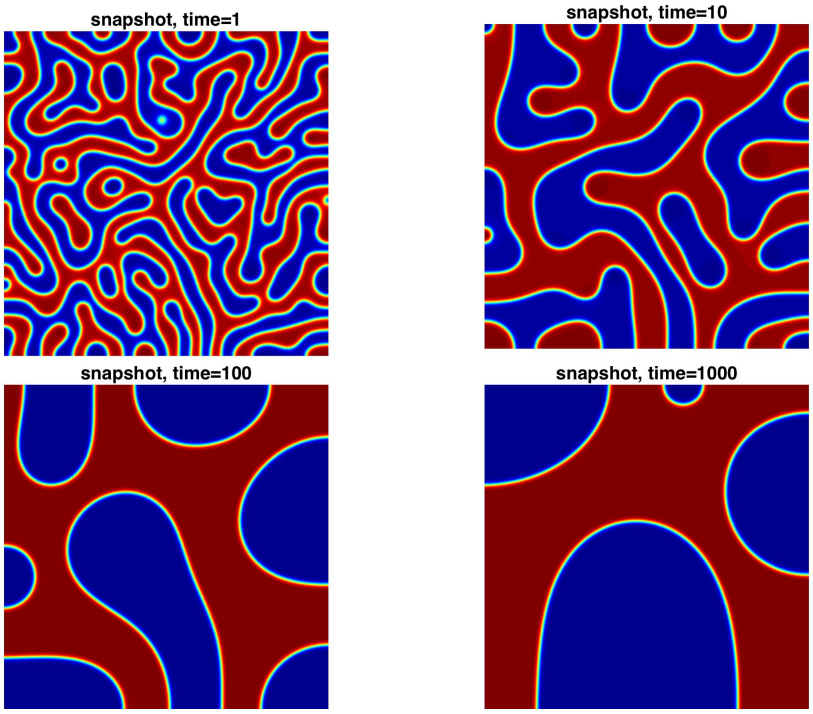

FIG. 6.3. *(Color online.) Snapshots of the computed phase variable ϕ at the indicated times for the parameters $L = 12.8$, $\varepsilon^2 = 0.005$.*

cal scheme by taking $\phi^{-1} = \phi^0$, with the initial data ϕ^0 given by the final time output of the last time period. Both the energy stability and second order numerical accuracy have been theoretically assured by our arguments in Theorems 4.1, 5.1, respectively. Figure 6.3 presents time snapshots of the phase variable ϕ with $\varepsilon^2 = 0.005$. A significant coarsening process is clearly observed in the system. At early times many small structures are present. At a later time, $t = 1000$, a single interface structure emerges, and further coarsening is not possible.

The long time characteristics of the energy decay rate is of interest to material scientists. To facilitate the energy scaling analysis, we add a constant $\frac{1}{4}|\Omega|$ to the energy introduced by (1.1):

$$\hat{E}(u) = \int_\Omega \left(\frac{1}{4}u^4 - \frac{1}{2}u^2 + \frac{1}{4} + \frac{\varepsilon^2}{2}|\nabla u|^2 \right) d\mathbf{x} = E(u) + \frac{1}{4}|\Omega|. \tag{6.3}$$

As a result, this energy is always non-negative. Figure 6.4 presents the log-log plot for the energy versus time, with the given physical parameter $\varepsilon^2 = 0.005$ and the artificial coefficient $A = \frac{1}{16}$. The detailed scaling "exponent" is obtained using least squares fits of the computed data up to time $t = 100$. A clear observation of the $a_e t^{b_e}$ scaling law can be made, with $a_e = 3.0018$, $b_e = -0.3463$. In other words, an almost perfect $t^{-1/3}$ energy dissipation law is confirmed by our numerical simulation.

Moreover, we preform a numerical test of this coarsening process with a bigger time step size and smaller value of A. Our numerical experiments show that, the physical energy still keeps decreasing even with a bigger time step size and $A < \frac{1}{16}$. In particular, Figure 6.5 gives the energy dissipation curve for $A = 0$ with larger time

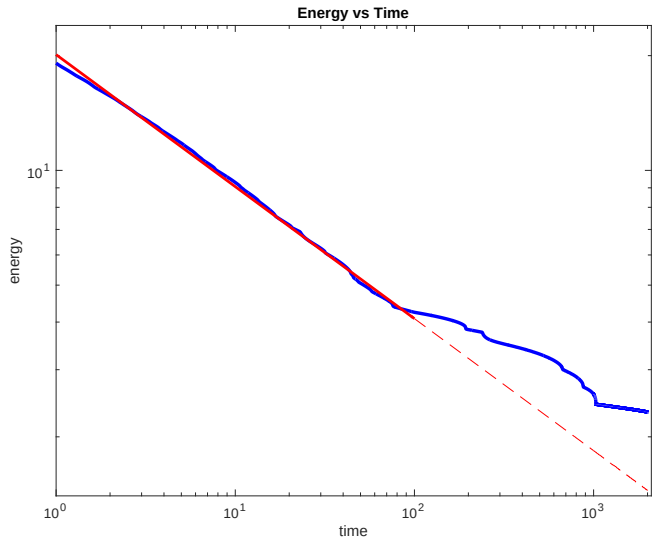

FIG. 6.4. *Log-log plot of the temporal evolution the energy E for $\varepsilon^2 = 0.005$. The energy decreases like $t^{-1/3}$ until saturation. The blue line represents the energy plot obtained by the simulation, while the red line is obtained by least squares approximations to the energy data. The least squares fit is only taken for the linear part of the calculated data, only up to about time $t = 100$. The fitted line has the form $a_e t^{b_e}$, with $a_e = 3.0018$, $b_e = -0.3463$.*

steps chosen at different coarsening process: $\tau = 0.04$ on the time interval $[0, 100]$, $\tau = 0.08$ on the time interval $[100, 2000]$. In this log-log plot, the slope of the least square fit line is -0.3222, which indicates a nice consistency with the $t^{-1/3}$ dissipation law.

These numerical simulation results have also provided many more insights on the proposed numerical scheme (2.2). Although a theoretical justification of the energy stability is only available with $A \geq \frac{1}{16}$, this numerical experiment has shown that such a constraint may only be a theoretical issue. Indeed, the numerical energy stability is often observed for any $A \geq 0$.

We make another observation that, although Figures 6.4 and 6.5 give almost exactly the same coarsening rate for the energy over time period [0,100], the numerical result displayed in Figure 6.4 seems to be more accurate, since the log-log oscillation over this time period is weaker than the one displayed in Figure 6.5. On the other hand, such a coarsening rate is only valid for short and medium time scale; after $t = 100$ (for a surface diffusion $\varepsilon^2 = 0.005$), the $t^{-1/3}$ coarsening rate may not be accurate any more, and the solutions are expected to converge to a steady state. Over the time period [100, 1000], we believe that the numerical results in Figure 6.4 are more accurate, due to the fact that the smaller time step sizes have been used to create this figure.

7. Concluding remarks. In this paper we have presented a second order BDF-type scheme for the Cahn-Hilliard equation (1.2), with a mixed finite element approximation in space. A unique solvability and unconditional energy stability (with a mild requirement $A \geq \frac{1}{16}$) turns out to be available. Moreover, such an energy estimate leads to a full order $O(\tau^2 + h^2)$ convergence analysis in the $\ell^\infty(0, T; L^2)$ norm.

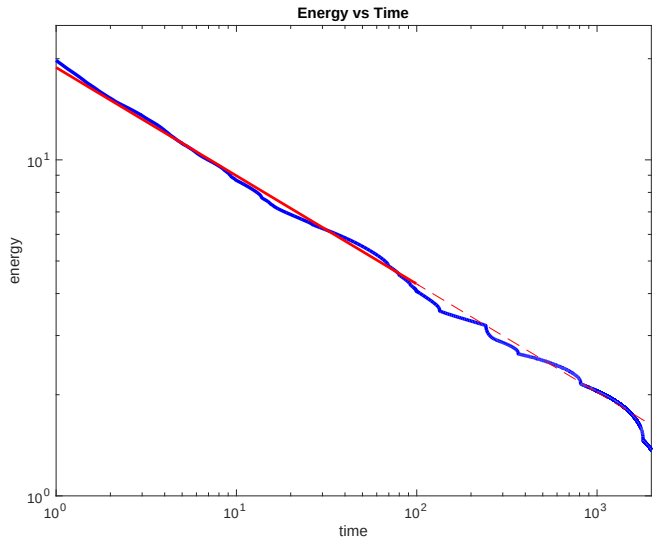

FIG. 6.5. *Log-log plot of the temporal evolution the energy E, with the same physical set-up as Figure 6.4. The artificial parameter is set as $A = 0$, and larger time steps are taken.*

In addition, the numerical experiment shows that the proposed second order BDF scheme is able to produce accurate long time numerical results with a reasonable computational cost. In particular, the energy dissipation rate given by the numerical simulation indicates an almost perfect match with the theoretical $t^{-1/3}$ prediction, which is remarkable.

Acknowledgment. This work is supported in part by the grants NSF DMS-1418689 (C. Wang), NSF DMS-1418692 (S. Wise), NSFC 11671098, 11331004, 91630309, a 111 project B08018 (W. Chen). Y. Yan thanks University of California-San Diego for support during her visit. C. Wang also thanks Shanghai Key Laboratory for Contemporary Applied Mathematics for support during his visit.

Appendix A. Proof of Proposition 5.1 .

Proof. We observe that

$$(u^{n+1})^3 - (u_h^{n+1})^3 = (u^{n+1})^3 - (R_h u^{n+1})^3 + (R_h u^{n+1})^3 - (u_h^{n+1})^3.$$

Therefore, we could separate the estimate of J_2 into two parts:

$$\begin{aligned} \|(u^{n+1})^3 - (R_h u^{n+1})^3\|^2 &= \| \left((u^{n+1})^2 + u^{n+1} R_h u^{n+1} + (R_h u^{n+1})^2\right) \rho^{n+1}\|^2 \\ &\le 8(\|u^{n+1}\|_\infty^4 + \|R_h u^{n+1}\|_\infty^4)\|\rho^{n+1}\|^2 \\ &\le C_{11} h^{2(q+1)} \|u^{n+1}\|_{H^{q+1}}^2, \end{aligned} \tag{A.1}$$

for some $C_{11} > 0$ that is independent of h and τ. The last estimate implies that

$$((u^{n+1})^3 - (R_h u^{n+1})^3, -\Delta_h \sigma_h^{n+1}) \le \frac{2C_{11} h^{2(q+1)}}{\varepsilon^2} \|u^{n+1}\|_{H^{q+1}}^2 + \frac{\varepsilon^2}{8} \|\Delta_h \sigma_h^{n+1}\|^2.$$

Define $\overline{u}_0 := \frac{1}{|\Omega|}(u_0, 1)$. Observe that $(R_h u^n - \overline{u}_0, 1) = (u_h^n - \overline{u}_0, 1) = 0$. In particular, $(\sigma_h^n, 1) = 0$, for all $n \ge 0$. We assume, as is standard, that $|\overline{u}_0| \le 1$. Now, for the

second part, we apply Hölder's inequality and use the embedding $H^1(\Omega) \hookrightarrow L^6(\Omega)$, and we get

$$\begin{aligned}
((R_h u^{n+1})^3 - (u_h^{n+1})^3, -\Delta_h \sigma_h^{n+1}) &\le \|(R_h u^{n+1})^3 - (u_h^{n+1})^3\| \cdot \|\Delta_h \sigma_h^{n+1}\| \\
&\le \|(R_h u^{n+1})^2 + R_h u^{n+1} u_h^{n+1} + (u_h^{n+1})^2\|_{L^3} \cdot \|\sigma_h^{n+1}\|_{L^6} \cdot \|\Delta_h \sigma_h^{n+1}\| \\
&\le 2\left(\|R_h u^{n+1}\|_{L^6}^2 + \|u_h^{n+1}\|_{L^6}^2\right) \cdot \|\sigma_h^{n+1}\|_{L^6} \cdot \|\Delta_h \sigma_h^{n+1}\| \\
&\le 4\left(\|R_h u^{n+1} - \overline{u}_0\|_{L^6}^2 + \|u_h^{n+1} - \overline{u}_0\|_{L^6}^2 + 2|\Omega|^{\frac{1}{3}}|\overline{u}_0|^2\right) \cdot \|\sigma_h^{n+1}\|_{L^6} \cdot \|\Delta_h \sigma_h^{n+1}\| \\
&\le 4C\left(\|\nabla R_h u^{n+1}\|^2 + \|\nabla u_h^{n+1}\|^2 + 2|\Omega|^{\frac{1}{3}}\right) \cdot \|\nabla \sigma_h^{n+1}\| \cdot \|\Delta_h \sigma_h^{n+1}\| \\
&\le 4C\left(\|\nabla u^{n+1}\|^2 + \|\nabla u_h^{n+1}\|^2 + 2|\Omega|^{\frac{1}{3}}\right) \cdot \|\nabla \sigma_h^{n+1}\| \cdot \|\Delta_h \sigma_h^{n+1}\| \\
&\le 4C\left(C + C_1 + 1\right) \cdot C\|\nabla \sigma_h^{n+1}\| \cdot \|\Delta_h \sigma_h^{n+1}\| \\
&\le C_{12}\|\sigma_h^{n+1}\|^{\frac{1}{2}} \cdot \|\Delta_h \sigma_h^{n+1}\|^{\frac{3}{2}},
\end{aligned} \tag{A.2}$$

for some $C_{12} > 0$ that is independent of τ and h. Next, we apply Young's inequality,

$$ab \le \frac{a^p}{p} + \frac{b^q}{q},$$

with $p = 4$ and $q = 4/3$. By carefully balancing the coefficients, we obtain

$$((R_h u^{n+1})^3 - (u_h)^3, -\Delta_h \sigma_h^{n+1}) \le \frac{54}{\varepsilon^6} C_{12}^4 \|\sigma_h^{n+1}\|^2 + \frac{\varepsilon^2}{8}\|\Delta_h \sigma_h^{n+1}\|^2.$$

This in turn yields inequality (5.33). The proof of Proposition 5.1 is complete. □

Appendix B. Proof of Proposition 5.2 .

Proof. For $n = 0$, inequality (5.31) indicates that

$$\begin{aligned}
\frac{1}{2}\|\sigma_h^1\|^2 + \frac{\tau\varepsilon^2}{2}\|\Delta_h \sigma_h^1\|^2 \le\ & \left(\frac{\tau}{2} + \frac{108\tau}{\varepsilon^6} C_{12}^4\right)\|\sigma_h^1\|^2 + 2Ch^{2(q+1)} \int_0^{t_1} \|\partial_t u\|_{H^{q+1}}^2 dt \\
&+ \frac{4Ch^{2(q+1)}}{\varepsilon^2}\tau\|w^1\|_{H^{q+1}}^2 + \frac{4}{\varepsilon^2} C_{11}\tau h^{2(q+1)}\|u^1\|_{H^{q+1}}^2 \\
&+ \frac{8C}{\varepsilon^2}\tau h^{2(q+1)}\|u^0\|_{H^{q+1}}^2 + \frac{4}{\varepsilon^2} Ch^{2(q+1)} \int_0^{t_1} \|\partial_t u\|_{H^{q+1}}^2 dt \\
&+ 4\tau^4 C_9 + 4\tau^4 C_{10}.
\end{aligned} \tag{B.1}$$

Equivalently,

$$\begin{aligned}
\frac{3}{2}\|\sigma_h^1\|^2 + \frac{\tau\varepsilon^2}{2}\|\Delta_h \sigma_h^1\|^2 \le\ & \tau\left(\frac{3}{2} + \frac{324}{\varepsilon^6} C_{12}^4\right)\|\sigma_h^1\|^2 + 6Ch^{2(q+1)} \int_0^{t_1} \|\partial_t u\|_{H^{q+1}}^2 dt \\
&+ \frac{12Ch^{2(q+1)}}{\varepsilon^2}\tau\|w^1\|_{H^{q+1}}^2 + \frac{12}{\varepsilon^2} C_{11}\tau h^{2(q+1)}\|u^1\|_{H^{q+1}}^2 \\
&+ \frac{24C}{\varepsilon^2}\tau h^{2(q+1)}\|u^0\|_{H^{q+1}}^2 + \frac{12}{\varepsilon^2} Ch^{2(q+1)} \int_0^{t_1} \|\partial_t u\|_{H^{q+1}}^2 dt \\
&+ 12\tau^4 C_9 + 12\tau^4 C_{10}.
\end{aligned} \tag{B.2}$$

Now, observe that $\left\|\mathbf{p}^1\right\|_{\mathsf{G}}^2 = \frac{3}{2}\left\|\sigma_h^1\right\|^2$ and $\left\|\mathbf{p}^{n+1}\right\|_{\mathsf{G}}^2 \geq \frac{1}{2}\left\|\sigma_h^{n+1}\right\|$. Summing (5.30) from $k=2$ to $k=n+1$, adding (B.2), and keeping in mind (5.3) (the relationship between G-norm and L^2-norm), we arrive at the following estimate for $n \geq 1$:

$$\begin{aligned}
&\frac{1}{2}\|\sigma_h^{n+1}\|^2 + \frac{\varepsilon^2\tau}{2}\sum_{k=0}^{n}\|\Delta_h\sigma_h^{k+1}\|^2 \leq \|\mathbf{p}^{n+1}\|_{\mathsf{G}}^2 + A\tau^2\|\Delta_h\sigma_h^{n+1}\|^2 + \frac{\varepsilon^2\tau}{2}\sum_{k=0}^{n}\|\Delta_h\sigma_h^{k+1}\|^2 \\
&\quad \leq \left(1 + \frac{108}{\varepsilon^6}C_{12}^4\right)\tau\|\sigma_h^{n+1}\|^2 + \left(\frac{3}{2} + \frac{324}{\varepsilon^6}C_{12}^4 + \frac{40}{\varepsilon^2}\right)\tau\sum_{k=0}^{n-1}\|\sigma_h^{k+1}\|^2 + \mathcal{R},
\end{aligned}$$

where

$$\begin{aligned}
\mathcal{R} &= h^{2(q+1)}\left(9C + \frac{12}{\varepsilon^2}\right)\int_0^T \|\partial_t u\|_{H^{q+1}}^2 dt + h^{2(q+1)}\cdot\frac{12C}{\epsilon^2}\tau\sum_{k=0}^{n}\|w^{k+1}\|_{H^{q+1}}^2 \\
&\quad + h^{2(q+1)}\frac{12C_{11}+40C}{\varepsilon^2}\tau\sum_{k=0}^{n}\|u^{k+1}\|_{H^{q+1}}^2 + \tau^4\cdot 64\int_0^T\|\partial_{ttt}u\|^2 dt \\
&\quad + \tau^4\cdot\frac{8}{\varepsilon^2}\left(32\int_0^T\|\partial_{tt}u\|^2 dt + A^2\int_0^T\|\partial_t\Delta u\|^2 dt\right) + 12\tau^4 C_9 + 12\tau^4 C_{10} \\
&\leq C_{13}(\varepsilon)(h^{2(q+1)} + \tau^4).
\end{aligned}$$

Under the time step requirement (5.35), which implies that

$$\begin{aligned}
\frac{1}{4}\|\sigma_h^{n+1}\|^2 + \frac{\varepsilon^2\tau}{4}\sum_{k=0}^{n}\|\Delta_h\sigma_h^{k+1}\|^2 \leq\ & \left(\frac{3}{2} + \frac{324}{\varepsilon^6}C_{12}^4 + \frac{40}{\varepsilon^2}\right)\tau\sum_{k=1}^{n}\|\sigma_h^k\|^2 \\
&+ C_{13}(\varepsilon)(h^{2(q+1)} + \tau^4).
\end{aligned}$$

Now, we can apply the discrete Gronwall inequality (5.1) and get

$$\|\sigma_h^{n+1}\|^2 + \varepsilon^2\tau\sum_{k=1}^{n+1}\|\Delta_h\sigma_h^k\|^2 \leq C_{15}(T,\varepsilon)(h^{2(q+1)} + \tau^4).$$

This completes the proof of Proposition 5.2. □

REFERENCES

[1] S. M. Allen and J. W. Cahn. A microscopic theory for antiphase boundary motion and its application to antiphase domain coarsening. *Acta. Metall.*, 27:1085, 1979.

[2] A. Aristotelous, O. Karakasian, and S.M. Wise. Adaptive, second-order in time, primitive-variable discontinuous Galerkin schemes for a Cahn-Hilliard equation with a mass source. *IMA J. Numer. Anal.*, 35:1167–1198, 2015.

[3] A. Baskaran, Z. Hu, J. Lowengrub, C. Wang, S.M. Wise, and P. Zhou. Energy stable and efficient finite-difference nonlinear multigrid schemes for the modified phase field crystal equation. *J. Comput. Phys.*, 250:270–292, 2013.

[4] A. Baskaran, J. Lowengrub, C. Wang, and S. Wise. Convergence analysis of a second order convex splitting scheme for the modified phase field crystal equation. *SIAM J. Numer. Anal.*, 51:2851–2873, 2013.

[5] B. Benešova, C. Melcher, and E. Süli. An implicit midpoint spectral approximation of nonlocal Cahn-Hilliard equations. *SIAM J. Numer. Anal.*, 52:1466–1496, 2014.

[6] S. Brenner and L. Scott. *The Mathematical Theory of Finite Element Methods*. Springer-Verlag, 3rd edition, 2010.

[7] J.W. Cahn and J.E. Hilliard. Free energy of a nonuniform system. i. interfacial free energy. *J. Chem. Phys.*, 28:258–267, 1958.

[8] W. Chen, S. Conde, C. Wang, X. Wang, and S.M. Wise. A linear energy stable scheme for a thin film model without slope selection. *J. Sci. Comput.*, 52:546–562, 2012.

[9] W. Chen, Y. Liu, C. Wang, and S.M. Wise. An optimal-rate convergence analysis of a fully discrete finite difference scheme for Cahn-Hilliard-Hele-Shaw equation. *Math. Comp.*, 85:2231–2257, 2016.

[10] W. Chen, C. Wang, X. Wang, and S.M. Wise. A linear iteration algorithm for energy stable second order scheme for a thin film model without slope selection. *J. Sci. Comput.*, 59:574–601, 2014.

[11] K. Cheng, C. Wang, S.M. Wise, and X. Yue. A second-order, weakly energy-stable pseudo-spectral scheme for the Cahn-Hilliard equation and its solution by the homogeneous linear iteration method. *J. Sci. Comput.*, 69:1083–1114, 2016.

[12] A. Christlieb, J. Jones, K. Promislow, B. Wetton, and M. Willoughby. High accuracy solutions to energy gradient flows from material science models. *J. Comput. Phys.*, 257:193–215, 2014.

[13] A. Diegel, X. Feng, and S.M. Wise. Convergence analysis of an unconditionally stable method for a Cahn-Hilliard-Stokes system of equations. *SIAM J. Numer. Anal.*, 53:127–152, 2015.

[14] A. Diegel, C. Wang, X. Wang, and S.M. Wise. Convergence analysis and error estimates for a second order accurate finite element method for the Cahn-Hilliard-Navier-Stokes system. *Numer. Math.*, 2017. accepted and in press.

[15] A. Diegel, C. Wang, and S.M. Wise. Stability and convergence of a second order mixed finite element method for the Cahn-Hilliard equation. *IMA J. Numer. Anal.*, 36:1867–1897, 2016.

[16] Q. Du and R. Nicolaides. Numerical analysis of a continuum model of a phase transition. *SIAM J. Numer. Anal.*, 28:1310–1322, 1991.

[17] D. Eyre. Unconditionally gradient stable time marching the Cahn-Hilliard equation. In J. W. Bullard, R. Kalia, M. Stoneham, and L.Q. Chen, editors, *Computational and Mathematical Models of Microstructural Evolution*, volume 53, pages 1686–1712, Warrendale, PA, USA, 1998. Materials Research Society.

[18] W. Feng, A.J. Salgado, C. Wang, and S.M. Wise. Preconditioned steepest descent methods for some nonlinear elliptic equations involving p-Laplacian terms. *J. Comput. Phys.*, 334:45–67, 2017.

[19] X. Feng and A. Prohl. Error analysis of a mixed finite element method for the Cahn-Hilliard equation. *Numer. Math.*, 99:47–84, 2004.

[20] X. Feng and S.M. Wise. Analysis of a fully discrete finite element approximation of a Darcy-Cahn-Hilliard diffuse interface model for the Hele-Shaw flow. *SIAM J. Numer. Anal.*, 50:1320–1343, 2012.

[21] D. Furihata. A stable and conservative finite difference scheme for the Cahn-Hilliard equation. *Numer. Math.*, 87:675–699, 2001.

[22] Z. Guan, J.S. Lowengrub, C. Wang, and S.M. Wise. Second-order convex splitting schemes for nonlocal Cahn-Hilliard and Allen-Cahn equations. *J. Comput. Phys.*, 277:48–71, 2014.

[23] Z. Guan, C. Wang, and S.M. Wise. A convergent convex splitting scheme for the periodic nonlocal Cahn-Hilliard equation. *Numer. Math.*, 128:377–406, 2014.

[24] F. Guillén-González and G. Tierra. Second order schemes and time-step adaptivity for Allen-Cahn and Cahn-Hilliard models. *Comput. Math. Appl.*, 68(8):821–846, 2014.

[25] J. Guo, C. Wang, S.M. Wise, and X. Yue. An H^2 convergence of a second-order convex-splitting, finite difference scheme for the three-dimensional Cahn-Hilliard equation. *Commu. Math. Sci.*, 14:489–515, 2016.

[26] D. Han, A. Brylev, X. Yang, and Z. Tan. Numerical analysis of second order, fully discrete energy stable schemes for phase field models of two phase incompressible flows. *J. Sci. Comput.*, 70:965–989, 2017.

[27] D. Han and X. Wang. A second order in time, uniquely solvable, unconditionally stable numerical scheme for Cahn-Hilliard-Navier-Stokes equation. *J. Comput. Phys.*, 290:139–156, 2015.

[28] Z. Hu, S. Wise, C. Wang, and J. Lowengrub. Stable and efficient finite-difference nonlinear-multigrid schemes for the phase-field crystal equation. *J. Comput. Phys.*, 228:5323–5339, 2009.

[29] L. Ju, X. Li, Z. Qiao, and H. Zhang. Energy stability and convergence of exponential time differencing schemes for the epitaxial growth model without slope selection. *Math. Comp.*, 2017. Accepted and in press.

[30] D. Li and Z. Qiao. On second order semi-implicit Fourier spectral methods for 2d Cahn-Hilliard

equations. *J. Sci. Comput.*, 70:301–341, 2017.
[31] D. Li, Z. Qiao, and T. Tang. Characterizing the stabilization size for semi-implicit Fourier-spectral method to phase field equations. *SIAM J. Numer. Anal.*, 54:1653–1681, 2016.
[32] J. Shen, C. Wang, X. Wang, and S.M. Wise. Second-order convex splitting schemes for gradient flows with Ehrlich-Schwoebel type energy: Application to thin film epitaxy. *SIAM J. Numer. Anal.*, 50:105–125, 2012.
[33] J. Shen, X. Yang, and H. Yu. Efficient energy stable numerical schemes for a phase field moving contact line model. *J. Comput. Phys.*, 284:617–630, 2015.
[34] C. Wang, X. Wang, and S.M. Wise. Unconditionally stable schemes for equations of thin film epitaxy. *Discrete Contin. Dyn. Sys. A*, 28:405–423, 2010.
[35] C. Wang and S.M. Wise. An energy stable and convergent finite-difference scheme for the modified phase field crystal equation. *SIAM J. Numer. Anal.*, 49:945–969, 2011.
[36] S.M. Wise. Unconditionally stable finite difference, nonlinear multigrid simulation of the Cahn-Hilliard-Hele-Shaw system of equations. *J. Sci. Comput.*, 44:38–68, 2010.
[37] S.M. Wise, C. Wang, and J.S. Lowengrub. An energy stable and convergent finite-difference scheme for the phase field crystal equation. *SIAM J. Numer. Anal.*, 47:2269–2288, 2009.
[38] X. Wu, G.J. van Zwieten, and K.G. van der Zee. Stabilized second-order convex splitting schemes for Cahn-Hilliard models with application to diffuse-interface tumor-growth models. *Inter. J. Numer. Methods Biomed. Eng.*, 30:180–203, 2014.
[39] X. Yang. Linear, and unconditionally energy stable numerical schemes for the phase field model of homopolymer blends. *J. Comput. Phys.*, 302:509–523, 2016.
[40] X. Yang and D. Han. Linearly first- and second-order, unconditionally energy stable schemes for the phase field crystal model. *J. Comput. Phys.*, 330:1116–1134, 2017.
[41] J. Zhao, Q. Wang, and X. Yang. Numerical approximations for a phase field dendritic crystal growth model based on the invariant energy quadratization approach. *Inter. J. Num. Meth. Engr.*, 110:279–300, 2017.